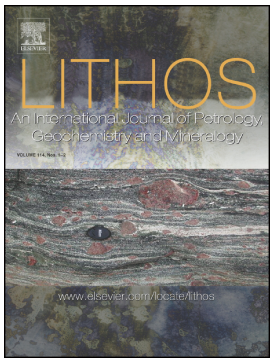
CORA Cork Open Research Archive
Cartlann Taighde Oscailte Chorcaí

Title	Chemical and isotopic changes induced by pyrometamorphism in metasedimentary xenoliths at Tongariro volcano, New Zealand
Authors	Pure, Leo R.;Charlier, Bruce L. A.;Wilson, Colin J. N.;Gamble, John A.;Vry, Julie K.;Townsend, Dougal B.;Leonard, Graham S.
Publication date	2021-08-04
Original Citation	Pure, L. R., Charlier, B. L. A., Wilson, C. J. N., Gamble, J. A., Vry, J. K., Townsend, D. B. and Leonard, G. S. (2021) 'Chemical and isotopic changes induced by pyrometamorphism in metasedimentary xenoliths at Tongariro volcano, New Zealand', Lithos, 400, 106404 (18pp). https://doi.org/10.1016/j.lithos.2021.106404
Type of publication	Article (peer-reviewed)
Link to publisher's version	10.1016/j.lithos.2021.106404
Rights	© 2021, Elsevier B.V. All rights reserved. This manuscript version is made available under the CC BY-NC-ND 4.0 license. - https://creativecommons.org/licenses/by-nc-nd/4.0/
Download date	2026-11-06 19:45:27
Item downloaded from	https://hdl.handle.net/10468/11734

UCC
University College Cork, Ireland
Coláiste na hOllscoile Corcaigh

Journal Pre-proof



Chemical and isotopic changes induced by pyrometamorphism in metasedimentary xenoliths at Tongariro volcano, New Zealand

Leo R. Pure, Bruce L.A. Charlier, Colin J.N. Wilson, John A. Gamble, Julie K. Vry, Dougal B. Townsend, Graham S. Leonard

PII: S0024-4937(21)00440-0

DOI: https://doi.org/10.1016/j.lithos.2021.106404

Reference: LITHOS 106404

To appear in: *LITHOS*

Received date: 19 April 2021

Revised date: 17 July 2021

Accepted date: 31 July 2021

Please cite this article as: L.R. Pure, B.L.A. Charlier, C.J.N. Wilson, et al., Chemical and isotopic changes induced by pyrometamorphism in metasedimentary xenoliths at Tongariro volcano, New Zealand, *LITHOS* (2021), https://doi.org/10.1016/j.lithos.2021.106404

This is a PDF file of an article that has undergone enhancements after acceptance, such as the addition of a cover page and metadata, and formatting for readability, but it is not yet the definitive version of record. This version will undergo additional copyediting, typesetting and review before it is published in its final form, but we are providing this version to give early visibility of the article. Please note that, during the production process, errors may be discovered which could affect the content, and all legal disclaimers that apply to the journal pertain.

© 2021 Published by Elsevier B.V.

Journal Pre-proof

Chemical and isotopic changes induced by pyrometamorphism in metasedimentary xenoliths at Tongariro volcano, New Zealand

Leo R. Pure[a,b,*] leo.r.pure@tutamail.com, Bruce L. A. Charlier[a], Colin J. N. Wilson[a], John A. Gamble[a,c], Julie K. Vry[a], Dougal B. Townsend[d], Graham S. Leonard[d]

[a]School of Geography, Environment and Earth Sciences, Victoria University, PO Box 600, Wellington 6140, New Zealand

[b]Environment Approvals Division, Department of Agriculture, Water and the Environment, PO Box 787, Canberra 2601, Australia

[c]School of Biological, Earth and Environmental Science, University College Cork, Ireland

[d]GNS Science, Avalon Research Centre, PO Box 30368, Lower Hutt 5045, New Zealand

[*]Corresponding author.

ABSTRACT

Andesites erupted from Tongariro volcano, North Island, New Zealand contain feldspathic and quartzose xenoliths derived from basement rocks. New major oxide, trace element and Sr-Nd-Pb isotopic data indicate that both the Waipapa and Kaweka (meta)sedimentary terranes are represented in erupted xenoliths, rather than only the Kaweka terrane as previously thought. Xenolith mineral assemblages differ from their likely source materials, notably through the lack of white mica, illite, chlorite and quartz, which is reflected in contrasting chemical and isotopic compositions. Major and trace element data indicate that most xenoliths underwent bulk mass decreases of about 50% when pyrometamorphosed at temperatures of ~800-980 °C, similar to typical Tongariro magma temperatures of ~800-1000 °C. Bulk Eu concentrations were retained (in restitic plagioclase); however, other rare earth elements are commonly lower in xenoliths than in protoliths. In xenoliths, the $^{143}Nd/^{144}Nd$ ratios of protoliths were also retained, which indicates that xenoliths were derived from the Kaweka and Waipapa terranes in subequal amounts. Reductions in $^{87}Sr/^{86}Sr$ ratios by up to 0.003 in xenoliths, relative to their likely protoliths, were accompanied by decreases in Rb/Sr ratios from 0.1-0.8 down to <0.1, reflecting the dissolution of hydrous, Rb-rich minerals (white mica ± illite) with their radiogenic isotopic ingrowths liberated into surrounding andesitic magmas. Varied amounts of U/Pb, Th/Pb and Th/U fractionation demonstrably occurred between xenoliths and protoliths, but these are challenging to correlate with Pb isotopic fractionation that also occurred. One xenolith contains a vein of clinopyroxene, calcic plagioclase, silicic glass and graphite that formed when quartz + calcite veins were pyrometamorphosed. The vein-bearing xenolith possesses unusual chemical and

isotopic features, which include a negative Ce anomaly, La_N/Yb_N ~2 and high $^{143}Nd/^{144}Nd$ (0.51284), which are also reported for xenolithic material erupted at neighbouring Ruapehu volcano.

KEYWORDS: Fractionation, Metasedimentary, Pyrometamorphism, Andesite, Restite, Xenolith

1. INTRODUCTION

The presence of xenoliths in igneous rocks provides direct evidence that country rock assimilation contributes to the assembly of arc magmas (e.g. Gill, 1981). In turn, the idea that entrained country rocks are completely melted and chemically incorporated in arc magmas underpins thermochemical models of assimilation-fractional crystallisation (AFC) processes (DePaolo, 1981; Spera and Bohrson, 2004), even though intact xenoliths are abundant in arc volcanic and plutonic rocks (White and Chappell, 1977; Gill, 1981; Rudnick et al., 1986; Graham and Hackett, 1987; Knesel and Davidson, 1999; Petcovic and Grunder, 2003; Wolf et al., 2019). Some studies have quantified the percentage of each xenolith that survives the assimilation process (Cesare et al., 1997; Mariga et al., 2006), but have not examined associated changes in radiogenic isotopic compositions. For these reasons, it is unclear whether the overall assimilant composition is better approximated by the bulk composition or the composition of a partial melt derived from the country rock. This distinction is fundamentally important when modelling AFC processes.

To address this distinction, this study examines bulk chemical and isotopic relationships between basement xenoliths, their protoliths and their host magmas (as erupted volcanic rocks) from a typical andesitic arc stratovolcano: Tongariro, New Zealand. We describe 25 inclusions that were derived from country rocks (Table 1) and which are petrographically and chemically distinct from cognate xenoliths also present in the Tongariro magma system (Pure, 2020). We present chemical and isotopic data for 16 of these inclusions (Tables 2 and 3) and compare their chemical compositions with reference data for their host lavas (Hobden, 1997; Pure, 2020) and

basement rocks (Price et al., 2015) exposed to the west and east of the volcano. The aims are to (1) identify the provenance of the xenoliths, relative to regional basement materials, (2) examine whether or not bulk xenolith compositions have shifted relative to their protolithic compositions, and (3) determine if the net assimilant composition (sum of all molten and unmolten components) in Tongariro magmas is better approximated by the bulk composition or a partial melt composition of the country rock.

1.1. Geological setting

Tongariro is a ~350 kyr old composite andesite volcano in the southern Taupō Volcanic Zone (TVZ), central North Island, New Zealand (Wilson et al., 1995; Pure et al., 2020; Fig. 1). The TVZ is a continental, rifting volcanic arc linked to subduction of the Pacific Plate beneath the Indo-Australian Plate with a convergence rate of ~43 mm/yr at the latitude of Tongariro (Nicol et al., 2007). Extension across the zone is occurring at ~15 mm/yr in the northern TVZ (offshore), reducing to ~7 mm/yr in the region of Tongariro (Wallace et al., 2004; Beavan et al., 2016; Gómez-Vasconcelos et al., 2017; Villamor et al., 2017) and terminating ~40 km farther south (Fig. 1: Villamor and Berryman, 2006).

Journal Pre-proof

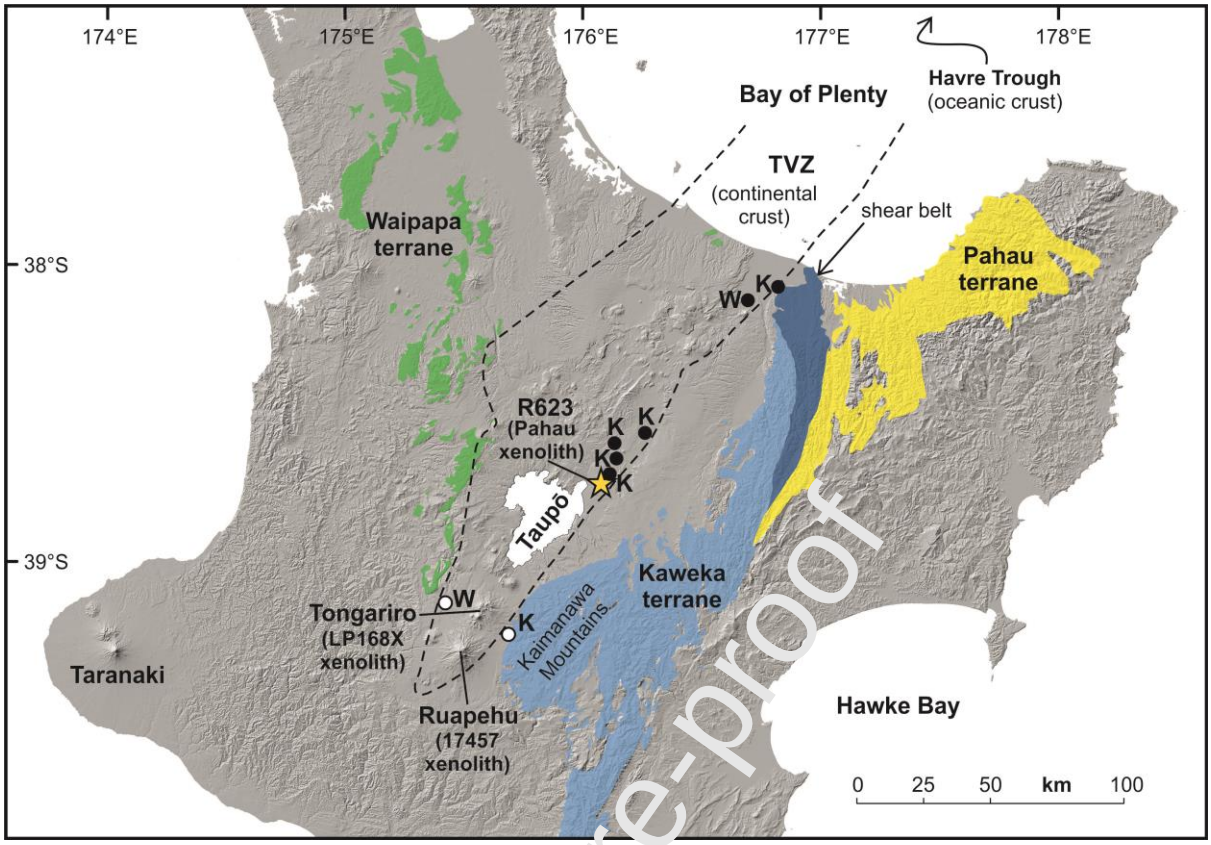


Fig. 1. Distributions of the Jurassic-Cretaceous Waipapa (green), Kaweka (light blue) and Pahau (yellow) terranes in the North Island of New Zealand, adapted from Charlier et al. (2010), Townsend et al. (2017) and Milicich et al. (2021). Dark blue shows a shear belt expressed within the Kaweka terrane. Black circles indicate drill hole sites which intercepted either Kaweka (K) or Waipapa (W) terrane rocks in the basement; Pahau terrane has not been encountered in drilling: open circles are from Beetham and Watters (1985); filled circles are from Milicich et al. (2021). Tongariro, Ruapehu, Taranaki and Taupō volcanoes are labelled. The dashed line shows the boundary of the Taupō Volcanic Zone (TVZ). Xenolith sample 17457 was erupted from Ruapehu (Graham, 1985); Pahau terrane xenolith R623 was erupted in the Rubbish Tip dome near Taupō (Sutton, 1995; Charlier et al., 2010); xenolith sample LP168X was erupted from Tongariro.

1.2. Basement geology of the southern TVZ

Previous studies suggested that the metasedimentary xenoliths in eruptives from Tongariro and adjacent volcanoes Ruapehu (to the south) and Taupō (to the north) could be derived from any of three juxtaposed Mesozoic greywacke-argillite terranes (Beetham and Watters, 1985; Charlier et al., 2010; Townsend et al., 2017). From oldest to youngest depositional age, these are the Waipapa composite terrane (Jurassic), and the Kaweka (Late Jurassic) and Pahau (Early Cretaceous) terranes within the Torlesse composite terrane (Mortimer, 1994; Mortimer et al., 2014).

At the surface, Waipapa terrane rocks occur ~15 km northwest of Tongariro in an uplifted fault block, where they are locally capped by <200 m of Neogene Māui Supergroup and Oligocene Te Kuiti Group rocks (Fig. 1) (Townsend et al., 2017). Waipapa rocks have also been intercepted at shallow depths (≤200 m) at sites ~10 km west of the Tongariro edifice (Beetham and Watters, 1985; Townsend et al., 2017). Rocks of the Kaweka terrane occur ~15 km east of Tongariro in the Kaimanawa Mountains. Results of zircon provenance studies on a metasedimentary xenolith (R623 in Fig. 1) erupted in a ~27 ka rhyolite dome indicate also that Pahau terrane rocks are present beneath the Taupō area (Sutton, 1995; Charlier et al., 2010), despite the fact that the nearest outcrops are ≥100 km to the northeast of Taupō and Tongariro. A review of intersected basement greywackes from geothermal drilling studies reported that both Kaweka and Waipapa terranes form the pre-volcanic basement beneath the central TVZ (Milicich et al., 2021). However, the geometry of the Waipapa-Kaweka terrane boundary beneath Tongariro is unclear from current geophysical data and rock structure data. Geophysical studies have suggested that metasedimentary basement rocks continue to depths of 15 km beneath Tongariro (Harrison and White, 2006; Bell et al., 2011; Stern and Benson, 2011). However, these studies can only broadly identify crustal lithologies from their seismic velocities, and the lithological contrasts between the Kaweka, Waipapa and Pahau have not been distinguished in seismic profiling.

Quaternary volcanic rocks in the southern TVZ are separated from the Mesozoic metasedimentary rocks by non-metamorphosed Neogene marine rocks with thicknesses of ≤1.5 km (Sissons and Dibble, 1981; Robertson and Davey, 2018) but these are largely buried by volcaniclastic sediments of the ring plain around Tongariro (Cronin and Neall, 1997; Townsend et al., 2017). At greater depths, the Mesozoic metasediments are proposed to rest on lower-crustal meta-igneous oceanic crust; however, evidence supporting this interpretation is limited (Graham et al., 1990). No other geological units are expected to comprise basement rocks beneath Tongariro, and geophysical studies suggest that upper crustal basement lithologies are of

comparable type between Tongariro and Taupō (Harrison and White, 2006; Behr et al., 2011; Stern and Benson, 2011; Robertson and Davey, 2018). For these reasons, we focus here on comparisons between our basement xenolith data versus those taken from surficial exposures of Waipapa, Kaweka and Pahau terrane rocks reported by Price et al. (2015).

Journal Pre-proof

Table 1. Petrographic features of basement xenoliths from Tongariro.

Sample	Mass (g)	Minerals	Maximum crystal size (μm)	Petrographic features
LP018X	-	pl + alk fsp > px ~ ox-rpl > ox	500	Some ox-rpls non-parallel to foliation
LP022X	-	pl + alk fsp > px ~ ox	400	2 mm compositional layering; ox more abundant in px-rich layers
LP025X	-	pl + alk fsp > px > ox > gls	800	Compositional layering; gls adjacent to px, pl and alk fsp; ox coincides with px
LP030X	-	qtz	1000	Curvilinear crystal surfaces with subparallel fractures at edges
LP032X	-	pl + alk fsp > px ~ ox > ox-rpl > gls	300	Foliated; ox-rpl surrounded by pl + alk fsp
LP034X	-	pl + alk fsp > px > ox > bio > mlt > hcy	500	Strong composition layering; ox more abundant in px-rich and bio-rich layers
LP063X	3.5	qtz	1200	Curvilinear crystal surfaces with subparallel fractures at edges
LP134X	11.2	pl + alk fsp > ox > px > mlt	300	Feldspars have two populations: pristine vs. partially internally dissolved
LP147X	8.6	pl + alk fsp > ox > px > ox-rpl	500	Crystal sizes in layers vary between 50-200 μm and 100-500 μm; some layers contain 40% Fe-Ti oxides
LP155X	7.1	pl + alk fsp > px ~ ox	600	Recrystallisation has overprinted any previous foliation
LP168X	4.7	host: pl + alk fsp > px ~ ox vein: pl, px, ox, mlt/gls, gph	200	Fine grained, foliated grey/black xenolith containing yellow-white vein
LP181X	1.6	zst > pl > ox	700	Zoisite is mottled/corroded and co-occurs with plagioclase
LP182X	1.3	n.t.s.	-	-
LP186X	1.5	n.t.s.	-	-
LP187X	1.4	pl > px > ox > ox-rpl	600	Anhedral crystal surfaces are slightly rounded; ox-rpls have ovular shapes
LP202X	0.3	pl + alk fsp > ox > gls	1200	Brown glass between anhedral pl crystals and within alk fsp as melt inclusions
LP204X	3.1	pl > alk fsp > ox > px > gls > bio	600	~1 mm layering; ox-rpl generally coincides with bio; gls common
LP205X	0.10	pl ~ px ~ ox ~ ox-rpl	200	Up to 1 mm ox-rpls orientated parallel to foliation direction
LP214X	3.0	pl > ox > px	500	~1 mm layering, ~700 μm ox-rpls; crystals isometric with rounded surfaces
LP215X	13.0	pl > alk fsp > ox > px > bio	1000	~1 mm layering, crystals more rounded on xenolith edges; bio in interior
LP233X	0.6	pl + alk fsp > ox > gls > px	500	~1-2 mm compositional and crystal size layering; 100-400 μm ox-rpls
LP234X	-	pl + alk fsp > px > ox > bio > cdm + tml	900	Layering poorly defined but foliated; px species is opx; trace cdm and tml
LP242X	0.3	pl + alk fsp > px > ox	500	Px is generally larger (100-400 μm) than pl and alk fsp (<40-100 μm)
LP245X	0.6	pl + alk fsp > ox > gls > ox	500	~1 mm layers; ≤1.5 mm ox-rpls
TG088X	0.1	n.t.s.	-	-

qtz = quartz, pl = plagioclase, alk fsp = alkali feldspar, px = pyroxene, cpx = clinopyroxene, opx = orthopyroxene, ox = Fe-Ti oxides, ox-rpl = Fe-Ti oxide replacement of pre-existing mineral, zst = zoisite, bio = biotite, gls = brown glass, mlt = devitrified melt, gph = graphite, cdm = corundum, tml = tourmaline, hcy = hercynite, n.t.s. = no thin section available for this sample, GM = groundmass. Trace minerals (zircon and apatite) are not included in this summary. Masses only recorded for xenoliths analysed compositionally. Foliation is relict from original protoliths and not imposed during magma ascent. Sample coordinates, host lava ages and stratigraphy are given the supplementary materials.

Journal Pre-proof

Journal Pre-proof

1.3. Previous work

Previous studies of Tongariro basement xenoliths by Graham (1987), Graham et al. (1988) and Hobden (1997, re-analysed by Price et al., 2010), are limited to samples from the 1954 to 1975 pyroclastic flow deposits and lavas erupted from the Ngāuruhoe vent. In contrast, this study investigates xenoliths obtained from eruptives with ages of ~190 ka to the Holocene (Pure et al., 2020). Xenoliths from Ruapehu have been studied by Graham (1987), Graham and Hackett (1987), Graham et al. (1990) and Conway et al. (2018).

Xenolith studies by Graham (1985, 1987), Graham et al. (1988), Hobden (1997) and Price et al. (2010) provide data for whole-rock major oxide (X-ray fluorescence [XRF]) and trace element concentration (XRF, instrumental neutron activation analysis [INAA], inductively coupled plasma mass spectrometry [ICP-MS]) and Sr-Nd-Pb isotope ratios (thermal ionisation mass spectrometry [TIMS] and multi-collector [MC]-ICP-MS) for Tongariro xenoliths. Graham (1987) also reports results of electron probe microanalyses of some minerals in these xenoliths. Pb isotopic ratios of Tongariro xenoliths, analysed by TIMS, are reported by Hobden (1997) and were re-measured by MC-ICP-MS by Price et al. (2010). The latter data are preferred for comparisons here because the earlier TIMS Pb data of Hobden (1997) were externally corrected for instrumental mass fractionation and hence are of lower precision.

2. ANALYTICAL METHODS

Basement xenoliths were cut from the fresh, unweathered interiors of samples from their host lavas or pyroclasts using a diamond saw. Where cut xenoliths were larger than 1 cm^2, one half was kept for micro-analytical study and the other half was powdered by hand using a clean agate mortar and pestle. XRF measurements of major oxide concentrations were performed at the University of Waikato (Hamilton, New Zealand) on fused 12:22 lithium tetraborate (35.3%) and lithium metaborate (64.7%) glass discs (0.8 g sample; 8.0 g flux). Analytical precision and accuracy were monitored using AGV-2 and BHVO-2 USGS rock standards, as well as an

internal standard (andesite lava sample LP009B: Pure, 2020). Analytical accuracy is within 3% (1 relative standard deviation [r.s.d.]) for each oxide except K_2O and P_2O_5 (within 5%, 1 r.s.d.), as indicated by comparisons with the recommended values of Jochum et al. (2016) and replicate analyses of sample LP009B.

Electron probe micro-analysis (EPMA) was used to identify minerals and quantitatively measure major oxide concentrations in xenolith glasses using a JEOL JXA-8230 Superprobe at Victoria University of Wellington (VUW). All EPMA analyses were performed at an accelerating voltage of 15 kV. Energy dispersive spectrometry (EDS) analyses were performed over 15-25 s with a beam current between 7.5 and 8.0 nA. Wavelength dispersive spectrometry (WDS) analyses of xenolith glasses were performed at beam currents of 2 nA (Si, Al, Fe, Ca, Na, K, P) and 8 nA (Ti, Mn, Mg) and quantified with a ZAF (atomic number-absorption-fluorescence) correction using JEOL software. Counting times were 15-20 s (background) and 30-60 s (peak) for all elements except Na (8 s [background]; 15 s [peak]). Replicate analyses of glass standards VG-A99 and VG-568 indicate that major oxide analyses are accurate to <5% (2 s.d.) for SiO_2 and <30% (2 s.d.) for all other oxides in concentrations above 0.5 wt%, but generally <15%.

For trace element and isotopic analyses xenolith powders were digested with 1 mL of concentrated HF and 50 μL of concentrated HNO_3 (20:1 ratio) per 50 mg of powder in sealed Teflon beakers at 120 °C overnight. Dried material was redissolved in 6M HCl then SiF_4 was evaporated at 120-140 °C repeatedly (at least twice) until a limpid solution was obtained. Trace element concentrations were measured on a Thermo Scientific Element II sector-field ICP-MS at VUW. Within-run uncertainties were typically 0.5-2.0% (1 r.s.d.), and external reproducibilities of AGV-2 and BHVO-2 (relative to the values reported by Jochum et al., 2016) were <1-9.2% (1 r.s.d.). Quadratic addition of weighing (0.04-0.20%, 1 r.s.d.) and measurement uncertainties yields an overall uncertainty of 1.4-10.5% (2 s.d.) except for Mo (≤12%), Cd (≤43%), In (≤49%), Sn (≤21%) and Tl (≤74%).

Journal Pre-proof

Sr-Nd-Pb isotopic compositions were measured using a ThermoFinnegan Triton TIMS at VUW. Digested samples were chemically purified to obtain Sr, Nd and Pb using the methods of Pin et al. (2014). Sr isotope analyses followed the methods of Charlier et al. (2006). Nd isotopic analyses were performed on double Re filaments loaded with 1-2 μL 0.1M H_3PO_4 which contained the purified samples. Samples prepared for Pb isotope analyses were leached in 6M HCl for 1 hr at 120 °C with the supernatant discarded. Pb isotopic measurements were performed on single Re filaments using an in-house ^{207}Pb-^{204}Pb double-spike method, after Thirlwall (2000). A full listing of the raw data is given in the supplementary materials. Replicate analyses (±2 s.d.) of recognised international solution standards gave NBS987 $^{87}Sr/^{86}Sr$ = 0.710267±17; JNdi-1 $^{143}Nd/^{144}Nd$ = 0.512105±8; NBS981 $^{206}Pb/^{204}Pb$ = 16.9422±29, $^{207}Pb/^{204}Pb$ = 15.5003±42, $^{208}Pb/^{204}Pb$ = 36.7281±98, $^{207}Pb/^{206}Pb$ = 0.91489±11 and $^{208}Pb/^{206}Pb$ = 2.16784±26. USGS standard AGV-2 gave $^{87}Sr/^{86}Sr$ = 0.703996±23, $^{143}Nd/^{144}Nd$ = 0.512772±8, $^{206}Pb/^{204}Pb$ = 18.9077±30, $^{207}Pb/^{204}Pb$ = 15.6154±43, $^{208}Pb/^{204}Pb$ = 38.5708±92, $^{207}Pb/^{206}Pb$ = 0.82588±12 and $^{208}Pb/^{206}Pb$ = 2.03995±21; BHVO-2 gave $^{87}Sr/^{86}Sr$ = 0.703508±23 and $^{143}Nd/^{144}Nd$ = 0.512977±9 (BHVO-2 not analysed for Pb isotopic compositions). To enable cross comparisons, all radiogenic isotope ratios, from this study and those previously published, were normalised to recommended values of NBS987 $^{87}Sr/^{86}Sr$ = 0.710248 (Thirlwall, 1991), JNdi-1 $^{143}Nd/^{144}Nd$ = 0.512115 (Tanaka et al., 2000) which is equivalent to La Jolla $^{143}Nd/^{144}Nd$ = 0.511858 (Lugmair and Carlson, 1978); NBS981 $^{206}Pb/^{204}Pb$ = 16.9409, $^{207}Pb/^{204}Pb$ = 15.4956, $^{208}Pb/^{204}Pb$ = 36.7228, $^{207}Pb/^{206}Pb$ = 0.91469, $^{208}Pb/^{206}Pb$ = 2.1677 (Thirlwall, 2000). When normalised with this scheme, USGS AGV-2 and BHVO-2 isotopic compositions are within analytical error of those reported by Raczek et al. (2003) (Sr and Nd) and Todd et al. (2015) (Pb; leached). All geochemical data are reported with quadratically combined internal (2 s.e.) and external reproducibilities (2 s.d.), including USGS standard data above, except where noted otherwise.

3. RESULTS

3.1. Textures and petrography

The textures and mineralogical characteristics of xenoliths are described in Table 1 and representative photographs are in Figs. 2 and 3. Xenolith masses are relatively small, ranging from 13.0 g down to 0.1 g. The 25 xenoliths studied generally have high aspect ratios (length:width >3) that are elongated in the direction of their internal foliation. Of these, 23 possess gneissic fabrics and are feldspar-rich whereas two xenoliths (LP030X and LP063X) are pure quartzites (Table 1; Figs. 2, 3). Quartzite xenoliths are most commonly observed in the field in eruptives with elevated MgO concentrations; however, both quartzite and feldspathic varieties commonly occur together in the same eruptive units. One xenolith (LP168X) is fine-grained (<200 μm) and contains a yellow-white coloured vein that comprises about 20 vol% of the clast (Figs. 2d, 3d, 3e).

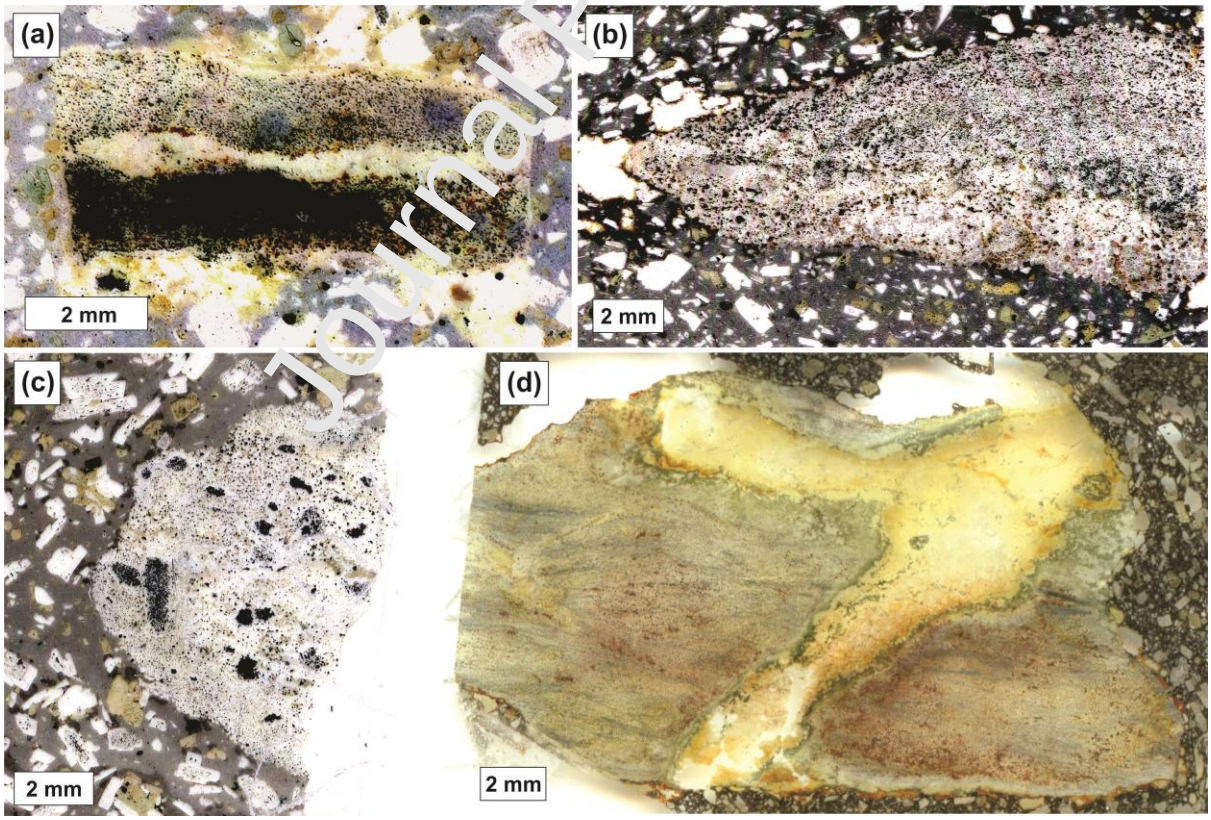


Fig. 2. Images from thin sections of representative basement xenoliths showing relationships with host lavas. Note that minerals generally align with the direction of foliation, and that textures are predominantly gneissic. **(a)** LP034 (207-200 ka Toatoa Member). **(b)** LP022 (102-96 ka Te Porere

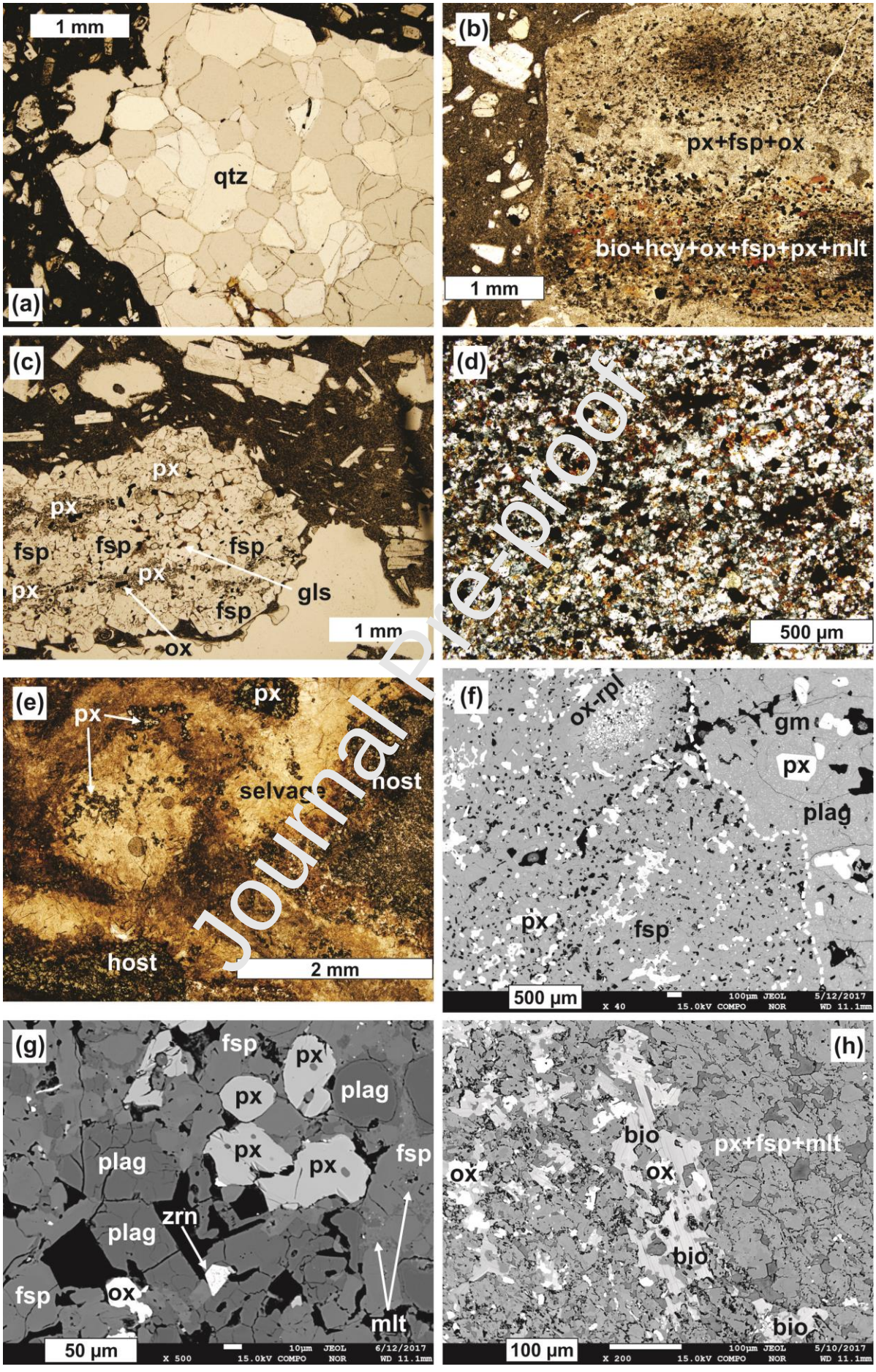
Journal Pre-proof

Member). **(c)** LP018 (96-92 ka Otamangakau Member). **(d)** LP168 (189-130 ka Te Pakiraki Member). For definitions of stratigraphic units, see Pure et al. (2020).

(Next page)

Fig. 3. Petrographic features of xenoliths. Stratigraphic nomenclature of host lavas from Pure et al. (2020). **(a)** Plane polarised light (PPL) image of pure quartz (qtz) xenolith LP030X (96-92 ka Otamangakau Member). **(b)** PPL image of LP034X (207-200 ka Toatoa Member). Note the 0.5-1.0 mm compositional layering and the orange biotite (bio). Opaque minerals are Fe-Ti oxides (ox) and spinels. Pyroxene (px), feldspar (fsp), hercynite (hcy) and devitrified melt (mlt) are also present. See also panel (h). **(c)** PPL image of LP025X (102-96 ka Te Porere Member). Note the 0.5-1.0 mm thick compositional layering of feldspar (fsp) and pyroxene (px). Brown glass (gls) occurs at rounded crystal interfaces. **(d, e)** PPL images of LP168X (189-130 ka Te Pakiraki Member). Panel (d) is a zoomed image of 'host' material labelled in panel (e). Opaque minerals are Fe-Ti oxides and spinels; brown material is pyroxene and oxidised Fe-minerals; light/transparent minerals are feldspars. **(f)** SEM back-scattered electron (BSE) image of LP032X (96-92 ka Otamangakau Member). Note the oval shaped cluster of Fe-Ti oxides (ox rpl: see Table 1) aligned with the foliation direction. The white line shows the xenolith-host contact. Pyroxene (px), plagioclase (plag), alkali feldspar (fsp) and lava groundmass (gm) are labelled. **(g)** BSE image of LP134X (33-23 ka Te Wai Whakaata Member) showing zircon (zrc), devitrified melt (mlt), pyroxene (px), alkali feldspar (fsp), plagioclase (plag) and Fe-Ti oxides (ox). **(h)** BSE image of LP034X (207-200 ka Toatoa Member) showing biotite (bio) and Fe-Ti oxides (ox). Pyroxene (px), devitrified melt (mlt), feldspar (fsp) and hercynite (hcy) also occur in this xenolith.

Journal Pre-proof



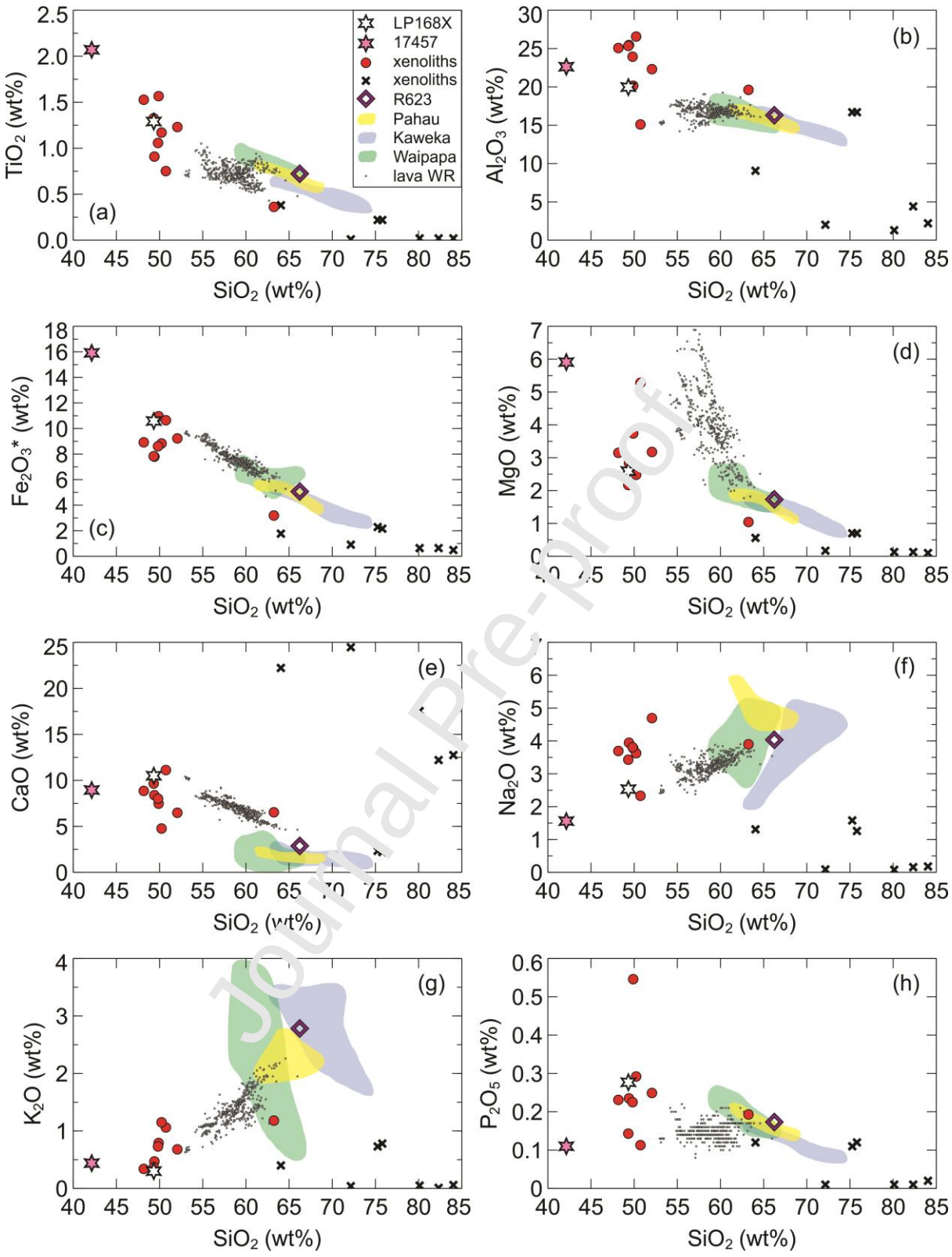
Journal Pre-proof

Mineral layering in gneissose xenoliths occurs in 0.5-2.0 mm bands (Table 1; Figs. 2, 3). Mineral grains are typically anhedral and sometimes trap pockets of brown glass (or its devitrified remains) between neighbouring crystals (Fig. 3c, g, h). When plagioclase occurs in xenoliths, it is almost always the most abundant mineral and is commonly accompanied by alkali feldspar (Table 1). Fe-Ti oxides are ubiquitous, always as magnetite and occasionally with ilmenite. Fe-Ti oxides are abundant in pyroxene-rich and biotite-rich layers but are rare in feldspar-rich layers. Pyroxene and Fe-Ti oxides occur in subequal proportions in most xenoliths (Fig. 3b). Some xenoliths contain ovoid clusters of magnetite, ilmenite and an unidentified opaque mineral (possibly a spinel group mineral), collectively denoted 'ox-rpl' in Table 1. These are inferred to represent areas of mineral replacement (Fig. 3f). The precursor mineral groups are likely to have formed part of the protolithic assemblage because elongated oxide clusters are typically aligned with the foliation in their host xenolith (Figs. 2c, 3f). Grain size heterogeneity is the greatest in xenoliths that contain uncommon minerals such as biotite, zoisite, tourmaline, corundum and hercynite (Table 1; Fig. 3b). Hydrous minerals are rare, only occurring as zoisite in sample LP181X. Brown-orange-red biotite is observed in four samples (Table 1; Fig. 3b, h) but is probably F-rich in the -OH lattice position because of pyrometamorphic changes that occur in biotite at andesitic temperatures (Munoz and Ludington, 1974). Xenoliths contain distinctly finer-grained apatite (<50 μm in LP134X and LP147X) than is observed in host andesites (typically ≤200 μm: Hobden, 1997; Pure et al., 2020). Zircon is absent as a phenocrystic or xenocrystic phase in host andesites, but occurs in trace amounts as ≤20 μm grains in some xenoliths (Fig. 3g).

One xenolith (LP168X) is cut by a vein of white and yellow material (Fig. 2d). The xenolith host material comprises 5-100 μm grains of plagioclase (~An_{50}), clinopyroxene (augite) and Fe-Ti oxides (one analysed crystal was $Mt_{40}Usp_{60}$: see supplementary materials) (Fig. 3d). At the host-selvage interface there are <100 μm crystals of anorthite, clinopyroxene (hedenbergite, augite and pigeonite), Fe-Ti oxides and graphite (Fig. 3e). The vein consists mostly of fibrous

153 yellow and white material could not be identified because the grain sizes were smaller than the
154 EPMA beam excitation area (~20 μm). However, intact ~100 μm anhedral crystals within the
155 vein could be identified as clinopyroxene (hedenbergite), although other pyroxenes may also be
156 present.
157
158 **3.2. Major oxides**
159 Xenoliths and metasedimentary rock (basement) reference samples fall into distinct
160 compositional groups with major oxide concentrations (Fig. 4). All xenoliths from this study,
161 except for pure quartzite xenoliths (not analysed) and LP134Y, have SiO_2 <55 wt% whereas the
162 reference samples have 59 to 75 wt% SiO_2 (Table 2; Fig. 4. Price et al., 2015). Relative to the
163 reference samples (Price et al., 2015), other oxide abundances in xenoliths are higher by ~5 wt%
164 for Al_2O_3, CaO, Fe_2O_3 and MgO, but are similar for Na_2O (~2-5 wt%) and P_2O_5 (~0.1-0.3 wt%)
165 (Fig. 4). In contrast, K_2O concentrations in xenoliths (~0-1.5 wt%) are lower than in reference
166 samples (~1-4 wt%: Price et al., 2015) and lava whole-rock samples (~1-2 wt%) (Fig. 4g).
167 However, interstitial brown glasses in the xenoliths contain 1-4 wt% K_2O, similar to the
168 reference and lava samples (see supplementary materials).
169 Two EDS raster (1.5 mm^2) analyses on xenolith LP168X show that the major oxide
170 composition of the host material, away from the vein, is similar to the bulk composition (host
171 xenolith plus vein) determined by XRF (Table 2). Relative to the host material, vein material is
172 more silicic. White vein material is richer in SiO_2 (73-85 wt%), TiO_2, CaO, Na_2O and K_2O
173 (5-6 wt%) than yellow vein material which is richer in FeO, MgO, MnO and contains Al_2O_3 (see
174 supplementary materials). The vein material is therefore similar to most xenoliths reported by
175 Price et al. (2010) that have >75 wt% SiO_2 and elevated CaO (>10 wt%) and which are quartz-
176 rich (Hobden, 1997).

Journal Pre-proof



177

178 **Fig. 4.** Major oxide variation diagrams for xenoliths and host lava samples from Tongariro. Xenolith data
179 are from this study (red filled circles) and Price et al. (2010: black crosses; all from the 1975 Ngāuruhoe
180 pyroclastic flow deposits). Reference data for possible correlative basement metasedimentary rocks are
181 from Price et al. (2015), and for Rubbish Tip dome at Taupō volcano (sample R623) from Sutton (1995).
182 Xenolith samples LP168X (this study: see text) and 17457 from Ruapehu (Graham, 1995; Lee, 2008) are
183 plotted as stars. Whole-rock (WR) lava data (small dots) are from Hobden (1997) and Pure (2020). All

184 oxides are normalised to 100% anhydrous totals and 2 s.d. uncertainties are approximately contained
185 within the symbols. Full xenolith data are in Table 2.
186

187 **Table 2.** Major oxide and trace element concentrations of basement xenoliths.

Sample	LP134X	LP147X	LP168X	LP181X	LP182X	LP186X	LP187X	LP202X
SiO_2 (wt%)	63.24	48.17	49.33	49.89	49.40	50.73	49.32	-
Al_2O_3	19.61	25.07	19.97	20.15	25.46	15.10	25.35	-
TiO_2	0.36	1.53	1.29	1.57	0.91	0.75	1.33	-
MnO	0.07	0.11	0.19	0.15	0.09	0.22	0.09	-
Fe_2O_3 total	3.19	8.92	10.59	10.96	7.80	10.65	7.83	-
MgO	1.04	3.15	2.59	3.74	2.84	5.28	2.17	-
CaO	6.53	8.86	10.50	7.47	8.39	11.12	9.65	-
Na_2O	3.90	3.69	2.53	3.78	3.95	2.33	3.43	-
K_2O	1.18	0.34	0.30	0.79	0.47	1.06	0.37	-
P_2O_5	0.19	0.23	0.28	0.55	0.24	0.11	0.14	-
LOI	0.20	-0.34	1.64	-0.35	0.11	2.97	0.71	-
Total	99.68	100.16	99.32	99.17	99.75	100.39	100.43	-
Sc (ppm)	6.86	22.1	41.8	31.8	13.3	36.9	11.0	12.6
V	53.1	218	312	248	149	322	289	202
Cr	3.15	103	695	102	57.6	154	91.7	55.1
Co	5.53	22.7	46.5	23.1	15.6	31.2	21.3	21.6
Ni	1.91	22.5	99.6	26.2	12.9	28.8	13.7	13.0
Cu	0.70	4.94	133	6.64	6.44	37.9	15.5	6.41
Zn	31.1	160	211	153	135	10	113	179
Ga	21.9	39.3	19.0	26.4	33.1	15	31.8	31.7
Rb	23.7	6.49	20.8	19.9	10.8	38.4	7.94	11.4
Sr	879	488	694	540	496	236	416	412
Y	27.0	20.9	51.2	46.4	22.5	25.8	6.46	10.3
Zr	39.0	46.4	64.1	71.7	28.3	62.1	27.5	34.6
Nb	5.12	19.3	2.37	20.2	10.86	2.59	5.33	5.70
Mo	0.20	0.48	1.50	0.59	0.41	0.74	0.30	0.29
Cd	0.03	0.06	0.11	0.06	0.03	0.14	0.04	0.03
In	0.01	0.03	0.05	0.04	0.02	0.05	0.02	0.02
Sn	-	-	1.27	1.11	0.75	1.37	0.73	0.56
Cs	0.37	0.96	4.63	1.17	1.72	1.40	0.59	0.99
Ba	513	320	116	614	371	184	147	181
La	24.2	40.0	12.6	53.2	37.6	11.0	7.31	13.9
Ce	49.9	80.5	33.1	115	77.5	22.0	13.7	27.6
Pr	5.96	8.81	4.58	13.5	8.83	2.84	1.62	3.25
Nd	24.6	34.1	22.7	52.9	32.6	12.0	6.39	12.8
Sm	4.74	6.27	6.52	10.9	6.14	3.03	1.27	2.51
Eu	1.15	1.7	1.76	2.3	1.82	0.84	0.99	1.22
Gd	4.53	5.75	7.45	10.4	5.82	3.43	1.32	2.52
Tb	0.68	0.78	1.28	1.54	0.77	0.58	0.19	0.34
Dy	4.03	4.21	8.27	8.62	4.12	3.81	1.08	1.88
Ho	0.85	0.80	1.74	1.67	0.78	0.82	0.23	0.37
Er	2.32	2.18	4.82	4.51	2.11	2.37	0.64	0.99
Tm	0.34	0.30	0.72	0.65	0.29	0.38	0.10	0.14
Yb	2.14	1.84	4.41	4.12	1.68	2.44	0.66	0.92
Lu	0.31	0.27	0.67	0.55	0.24	0.39	0.10	0.14
Hf	1.10	1.62	1.94	2.46	0.93	2.08	0.93	1.07
Ta	0.42	1.64	0.21	1.72	0.99	0.27	0.50	0.41
Tl	0.09	0.08	0.08	0.09	0.08	0.19	0.32	0.10
Pb	7.02	5.16	13.8	10.7	7.33	6.03	5.34	4.57
Th	3.01	11.5	0.19	19.5	10.7	2.90	0.91	2.29
U	0.55	0.92	0.34	3.00	1.25	0.71	0.22	0.35
Eu/Eu*	0.72	0.82	0.78	0.66	0.93	0.79	2.33	1.48

Journal Pre-proof

188 **Table 2.** (continued)

Sample	LP204X	LP205X	LP214X	LP215X	LP233X	LP242X	LP245X	TG088X
SiO_2 (wt%)	52.06	-	50.23	49.82	-	-	-	-
Al_2O_3	22.31	-	26.56	23.94	-	-	-	-
TiO_2	1.23	-	1.17	1.06	-	-	-	-
MnO	0.07	-	0.12	0.10	-	-	-	-
Fe_2O_3 total	9.23	-	8.83	8.61	-	-	-	-
MgO	3.18	-	2.48	2.77	-	-	-	-
CaO	6.48	-	4.77	8.02	-	-	-	-
Na_2O	4.69	-	3.63	3.81	-	-	-	-
K_2O	0.68	-	1.15	0.73	-	-	-	-
P_2O_5	0.25	-	0.29	0.23	-	-	-	-
LOI	0.27	-	1.29	0.23	-	-	-	-
Total	100.69	-	100.64	99.42	-	-	-	-
Sc (ppm)	22.5	12.0	20.4	17.5	13.2	22.9	12.1	23.6
V	195	231	211	191	165	180	174	302
Cr	61.6	61.1	81.7	68.8	52.6	45.3	65.9	115
Co	17.5	23.2	26.3	22.8	16.0	19.1	18.4	27.2
Ni	21.2	31.3	32.8	26.4	13.4	20.4	10.7	17.1
Cu	25.1	29.7	30.7	24.1	7.21	1095	1.13	7.58
Zn	168	99.4	183	164	86.6	134	144	100
Ga	32.6	31.3	37.8	36.9	34.5	19.0	29.4	26.0
Rb	19.2	17.8	31.4	22.4	10.3	15.4	14.9	4.71
Sr	620	482	505	456	510	385	434	400
Y	27.2	9.96	38.2	20.9	12.3	11.2	16.6	47.7
Zr	87.6	46.8	40.1	41.2	26.0	92.0	63.6	29.0
Nb	15.5	1.97	17.0	13.4	12.8	6.29	9.20	4.64
Mo	1.52	0.28	0.77	0.76	0.53	2.88	0.43	0.27
Cd	0.05	0.04	0.07	0.04	0.05	0.10	0.04	0.04
In	0.03	0.02	0.01	0.02	0.02	0.04	0.02	0.03
Sn	0.84	0.89	0.89	0.81	0.51	1.63	0.99	0.71
Cs	1.30	1.09	2.99	1.84	0.59	1.28	0.79	0.54
Ba	782	155	503	477	812	279	286	128
La	42.4	11.3	47.4	31.8	24.2	14.4	27.5	37.0
Ce	87.8	21.4	98.0	62.4	50.9	28.2	55.3	85.7
Pr	10.1	2.52	11.5	7.28	6.03	3.49	6.45	11.6
Nd	38.1	9.76	43.7	29.0	22.8	13.9	24.6	52.1
Sm	7.21	1.88	8.53	5.40	4.20	2.89	4.57	11.5
Eu	2.11	0.90	2.02	1.50	1.73	1.22	1.28	1.92
Gd	6.88	1.96	8.21	5.22	3.77	2.99	4.35	11.9
Tb	0.93	0.28	1.15	0.71	0.46	0.45	0.57	1.63
Dy	5.02	1.68	6.40	3.84	2.31	2.80	3.09	8.95
Ho	0.96	0.35	1.27	0.74	0.44	0.59	0.60	1.72
Er	2.61	0.96	3.43	1.99	1.21	1.68	1.63	4.31
Tm	0.37	0.15	0.48	0.27	0.17	0.27	0.23	0.55
Yb	2.24	0.97	2.78	1.65	1.08	1.77	1.44	3.14
Lu	0.32	0.15	0.40	0.24	0.16	0.29	0.22	0.44
Hf	2.67	1.47	1.59	1.34	1.19	2.69	1.77	0.93
Ta	0.87	0.16	1.09	0.91	1.00	0.41	0.66	0.43
Tl	0.14	0.12	0.31	0.14	0.09	0.13	0.09	0.06
Pb	10.4	4.15	19.2	6.23	6.13	67.2	6.47	4.61
Th	16.8	2.13	17.1	10.8	10.8	3.01	8.45	1.22
U	2.62	0.52	2.80	1.28	0.64	0.91	0.98	0.35
Eu/Eu*	0.91	1.43	0.74	0.86	1.33	1.27	0.88	0.50

189 Data are raw totals. Where plotted in Fig. 4, the data are normalised to 100% anhydrous totals. Some
190 xenoliths were not large enough for XRF analysis. Eu/Eu* was calculated as $Eu_N/(sqrt(Sm_N*Gd_N))$;
191 Ce/Ce* was calculated as $Ce_N/(sqrt(La_N*Pr_N))$ after normalisation with the CI chondrite values of
192 McDonough and Sun (1995).
193

Journal Pre-proof

194 **3.3. Trace elements**

195 Full trace element data for the xenoliths are reported in Table 2. These data are
196 compared with those for Waipapa, Kaweka and Pahau terranes and other xenoliths in Figs. 5 and
197 6 (Price et al., 2010, 2015). Overall, incompatible trace element concentrations are depleted in
198 xenoliths compared with the reference samples of Price et al. (2015). These chemical
199 relationships are described for parent-daughter elements of the Sr-Nd-Pb isotopic systems, as a
200 pre-requisite to evaluating isotopic differences between xenoliths and plausible protolithic
201 materials.

202 Bulk Rb/Sr ratios in xenoliths and basement reference samples are offset (Fig. 5: Price et
203 al., 2010, 2015). Generally lower Rb/Sr ratios in xenoliths (<0.1), relative to reference samples
204 (0.1-0.8), are controlled by contrasting Rb concentrations (Fig. 5a, b, c). Compared with
205 reference samples, xenoliths contain less Rb (5-38 versus 24-171 ppm) and Cs (0.3-6.5 versus
206 1.6-10.9 ppm) but have similar amounts of Sr (236-880 versus 159-723 ppm) and Ba (8-812
207 versus 150-1305 ppm) (Table 2; Fig. 5a, b, c).

208 Sm/Nd ratios in xenoliths and reference samples are similar, as are absolute Sm and Nd
209 concentrations (Table 2; Fig. 5d). Typical Sm/Nd values range from 0.18 to 0.28 for all sample
210 types (Table 2) which define an array with similar Sm/Nd to bulk continental crust (Fig. 5d)
211 (Rudnick and Gao, 2003).

212 Zr is strongly correlated with Hf in xenoliths, host lavas and reference samples that
213 together form a single, linear array with similar Hf/Zr to bulk continental crust (Fig. 5e)
214 (Rudnick and Gao, 2003). Xenoliths have distinctly lower Zr (26-88 versus 137-260 ppm) and Hf
215 (0.9-2.7 versus 3.5-8.3 ppm) than reference samples (Price et al., 2015). The gap between the
216 xenolith and reference sample Zr-Hf concentrations is bridged by host lavas and their interstitial
217 melts (represented by groundmass separates) that contain ~80-170 ppm Zr and ~2.5-4.5 ppm
218 Hf. One exception (xenolith TG267) has 232 ppm Zr and 5.3 ppm Hf that overlap with
219 reference sample Hf-Zr concentrations (Price et al., 2010).

Journal Pre-proof

Journal Pre-proof

220 Xenolith U/Pb, Th/Pb and Th/U ratios generally differ from reference samples (Fig. 5f,
221 g, h). Of 23 Tongariro xenoliths reported here and by Price et al. (2010), 14 have U/Pb ratios
222 that overlap with basement reference sample ratios of 0.08-0.20, however 9 other xenoliths occur
223 outside this range (Fig. 5f). Relatively greater offsets in Th/Pb and Th/U ratios occur between
224 basement samples and ~35% of all Tongariro xenoliths (Fig. 5g, h).

Journal Pre-proof

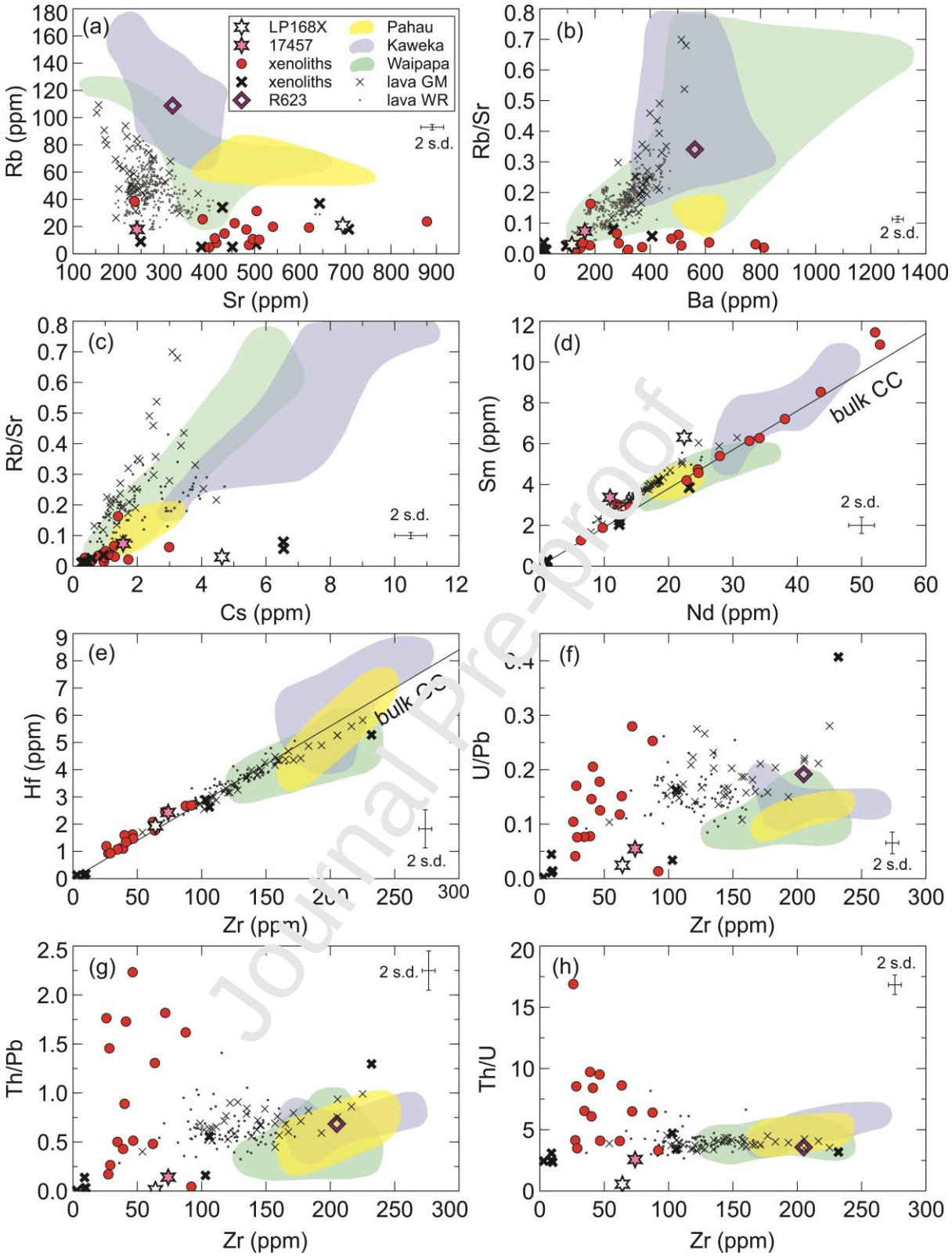


Fig. 5. Trace element variation diagrams for xenoliths from Tongariro. Xenolith data are from this study (red filled circles) and Price et al. (2010: black crosses; all from the 1975 Ngāuruhoe pyroclastic flow deposits). Reference data for possible correlative basement metasedimentary rocks are from Price et al. (2015) and include 2 s.d. errors. Other xenolith data are from Rubbish Tip Dome at Taupō volcano (sample R623: Sutton, 1995) and Ruapehu volcano (sample 17457: Graham, 1995; Lee, 2008). Whole-rock (WR) lava data are from Hobden (1997) and Pure (2020). Tongariro groundmass (GM) data are

from Pure (2020). 2 s.d. errors are shown. Full xenolith data are contained in Table 2. "Bulk CC" refers to bulk continental crust which has Sm/Nd = 0.19 and Hf/Zr = 0.028 (Rudnick and Gao, 2003).

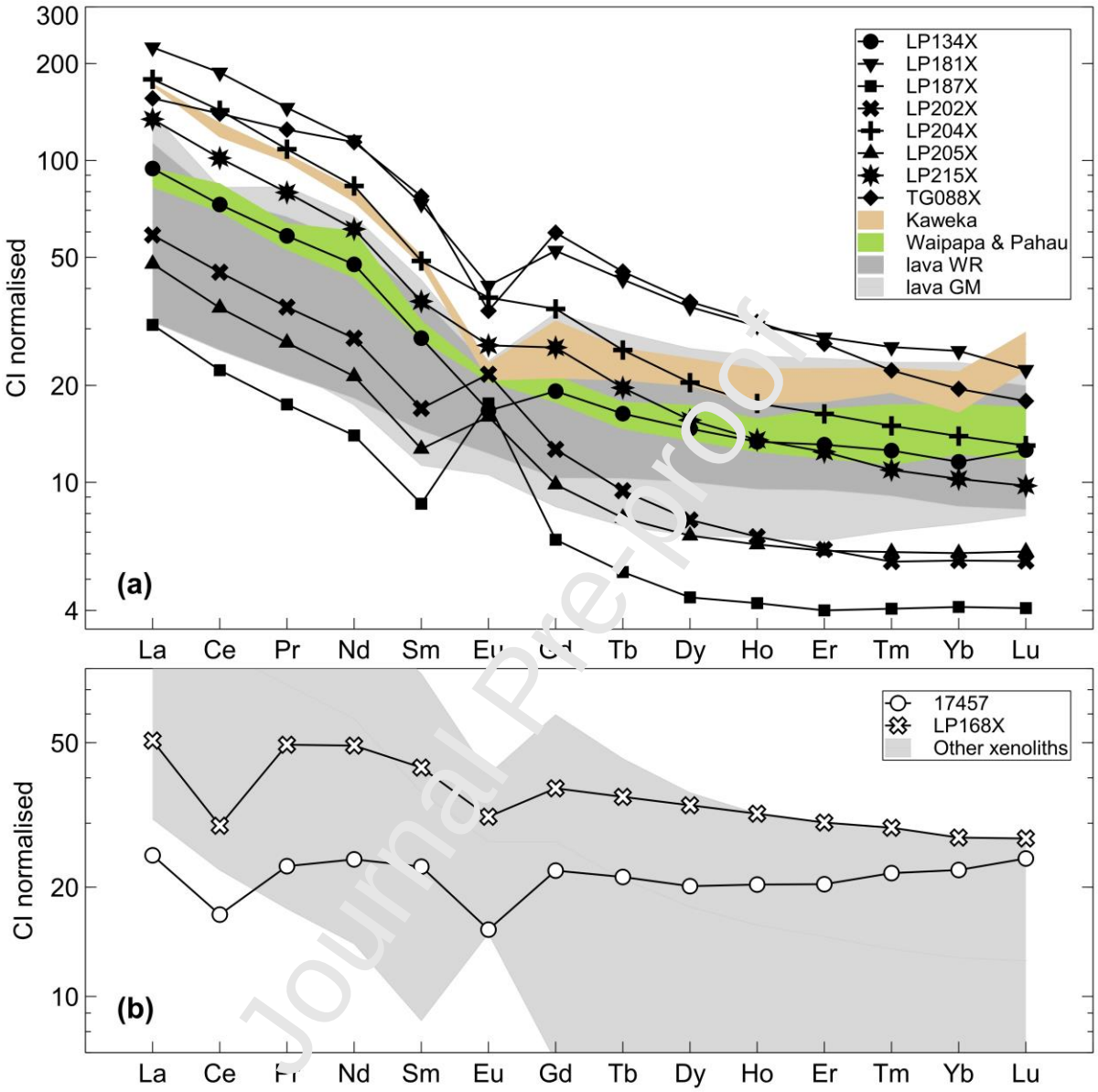


Fig. 6. Xenolith rare earth element (REE) diagrams. Concentrations normalised to the CI chondrite values of McDonough and Sun (1995). **(a)** Tongariro whole-rock (WR) and groundmass (GM) fields are defined from data in Pure (2020). Reference data for possible correlative basement terrane rocks are from Price et al. (2015). Pahau and Waipapa REE concentrations closely overlap so are not distinguished. Full xenolith data are contained in Table 2. **(b)** Comparisons between xenoliths LP168X and 17457 (Lee, 2008) with other xenoliths in this study.

245 Rare earth element (REE) concentrations of xenoliths reveal coupled variation in light
246 REE and heavy REE concentrations, with La_N/Yb_N values of ~4 to 10 (normalised to CI-
247 chondrite values: McDonough and Sun, 1995); however, Eu is relatively invariant (Fig. 6a). One
248 exception (xenolith LP168X, including the vein) has La_N/Yb_N ~2 and a negative Ce anomaly
249 (Fig. 6b), features that are absent in other xenoliths reported here or by Graham (1987), Graham
250 et al. (1988, 1990), Hobden (1997) and Price et al. (2010). We are only aware of these REE
251 features in one other sample (17457) from Ruapehu, collected by Graham (1985) and re-analysed
252 by Lee (2008).
253
254 **3.4. Sr-Nd-Pb isotopes**
255 Sr-Nd-Pb isotopic compositions of xenoliths show both similarities to and differences
256 from basement reference samples (Fig. 7). There is no unique correspondence between Sr-Nd
257 isotopic compositions in xenoliths and those from samples of the outcrops of the Pahau,
258 Kaweka or Waipapa terranes adjacent to the TVZ (Price et al., 2015). In Sr-Nd isotopic space,
259 xenolith and reference sample compositions diverge at values of high $^{87}Sr/^{86}Sr$ (>0.707) and low
260 $^{143}Nd/^{144}Nd$ (<0.5126) but otherwise overlap (Fig. 7a). Xenolith LP168X has an unusually high
261 $^{143}Nd/^{144}Nd$ ratio of 0.51284, similar to xenolith 17457 ($^{143}Nd/^{144}Nd$ = 0.51296) with which it
262 also shares atypical REE features (Fig. 6b) (Lee, 2008). Quartz-wollastonite-calcic plagioclase
263 xenoliths reported by Hobden (1997) and analysed by Price et al. (2010) have $^{87}Sr/^{86}Sr$ ratios of
264 0.70757 to 0.70817, and $^{143}Nd/^{144}Nd$ ratios of 0.51239 to 0.51277, similar to corresponding
265 xenoliths reported here.
266 Certain Pb isotope ratios in some xenoliths are uniquely similar to one of the Pahau,
267 Kaweka and Waipapa terranes (Fig. 7), yet other Pb isotopic ratios in other xenoliths do not
268 conform to any pattern. For example, xenolithic $^{206}Pb/^{204}Pb$ ratios (18.81-18.89) and $^{208}Pb/^{204}Pb$
269 ratios (38.72-38.83) are most similar to those of the Kaweka terrane (18.85-18.96 and 38.72-
270 38.84, respectively) (Fig. 7c). In contrast, xenolith $^{207}Pb/^{204}Pb$ ratios (15.61-15.65) generally plot

Journal Pre-proof

between the Kaweka (15.64-15.65), Waipapa (15.61-15.63) and Pahau (15.61-15.62) arrays (Fig. 7b). Likewise, xenolith $^{207}Pb/^{206}Pb$ ratios (generally 0.8288-0.8302) overlap with values from all three terranes, whereas xenolith $^{208}Pb/^{206}Pb$ ratios (generally 2.055-2.058) only overlap with Waipapa (~2.057-2.060) and Pahau ratios (~2.053-2.057: Fig. 7d). Sample LP168X has higher $^{207}Pb/^{206}Pb$ (2.0627) and $^{208}Pb/^{206}Pb$ (0.8323) ratios than other xenoliths analysed in this study but has similar Pb isotopic compositions to quartz-wollastonite-calcic plagioclase xenoliths collected by Hobden (1997) and analysed by Price et al. (2010), and also to the xenolith sample 17457 reported by Graham (1985) and Lee (2008) (Table 3; Fig. 7d).

Table 3. Sr-Nd-Pb isotope ratios of basement xenoliths.

Sample	$^{87}Sr/^{86}Sr$	$^{143}Nd/^{144}Nd$	$^{206}Pb/^{204}Pb$	$^{207}Pb/^{204}Pb$	$^{208}Pb/^{204}Pb$	$^{207}Pb/^{206}Pb$	$^{208}Pb/^{206}Pb$
LP134X	0.707199 ± 23	0.512748 ± 9	18.8303 ± 17	15.628[illegible] ± 2[illegible]	38.7396 ± 68	0.82997 ± 6	2.05730 ± 24
LP147X	0.706825 ± 23	0.512488 ± 9	18.8702 ± 33	15.6[illegible] ± [illegible]	38.7865 ± 97	0.82897 ± 12	2.05543 ± 21
LP168X	0.707761 ± 23	0.512835 ± 8	18.8085 ± 15	[illegible]544 ± 22	38.7965 ± 66	0.83231 ± 6	2.06271 ± 24
LP181X	0.708062 ± 23	0.512470 ± 9	18.8855 ± 16	[illegible]651 ± 23	38.8305 ± 69	0.82885 ± 7	2.05610 ± 24
LP182X	0.707823 ± 23	0.512427 ± 10	18.8760 ± 30	15.6473 ± 44	38.8017 ± 94	0.82895 ± 12	2.05561 ± 22
LP186X	0.705449 ± 23	0.512722 ± 9	18.8460 ± [illegible]	15.6309 ± 43	38.7539 ± 92	0.82940 ± 12	2.05634 ± 21
LP187X	0.705549 ± 4	0.512702 ± 9	18.846[illegible] ± 3[illegible]	15.6322 ± 44	38.7536 ± 94	0.82945 ± 12	2.05627 ± 21
LP202X	0.706155 ± 23	0.512559 ± 9	18.8522 ± [illegible]	15.6325 ± 22	38.7546 ± 68	0.82921 ± 6	2.05571 ± 24
LP204X	0.706367 ± 23	0.512558 ± 9	18.[illegible]632 ± 15	15.6447 ± 22	38.8053 ± 67	0.82938 ± 6	2.05720 ± 24
LP205X	0.705379 ± 23	0.512678 ± 9	18.831[illegible] ± 155	15.6332 ± 139	38.7429 ± 363	0.83015 ± 17	2.05732 ± 54
LP214X	0.708505 ± 37	0.512431 ± 10	18.8[illegible]5 ± 15	15.6468 ± 22	38.8067 ± 67	0.82956 ± 6	2.05745 ± 24
LP215X	0.705893 ± 23	0.512515 ± 8	18.[illegible]51[illegible] ± 30	15.6361 ± 43	38.7660 ± 92	0.82945 ± 12	2.05641 ± 21
LP233X	0.706794 ± 23	0.512496 ± 9	18.[illegible]8653 ± 30	15.6405 ± 43	38.7867 ± 92	0.82906 ± 12	2.05598 ± 21
LP242X	0.706845 ± 23	0.512611 ± 12	18.8448 ± 16	15.6297 ± 22	38.7537 ± 67	0.82939 ± 6	2.05647 ± 24
LP245X	0.706475 ± 23	0.512528 ± [illegible]	18.8548 ± 30	15.6339 ± 43	38.7668 ± 92	0.82918 ± 12	2.05607 ± 21
TG088X	0.705629 ± 23	0.512564 ± [illegible]	18.8339 ± 21	15.6180 ± 27	38.7177 ± 80	0.82925 ± 7	2.05575 ± 26

$^{87}Sr/^{86}Sr$ data normalised to NBS987 = 0.710248 after Thirlwall (1991). $^{143}Nd/^{144}Nd$ data normalised to JNdi-1 = 0.512115 (Tanaka et al. 2000) which is equivalent to La Jolla = 0.511858 after Lugmair and Carlson (1978). Pb isotope data normalised to NBS981 values of Thirlwall (2000): $^{206}Pb/^{204}Pb$ = 16.9409, $^{207}Pb/^{204}Pb$ = 15.4956, $^{208}Pb/^{204}Pb$ = 36.7228, $^{207}Pb/^{206}Pb$ = 0.91469 and $^{208}Pb/^{206}Pb$ = 2.1677.

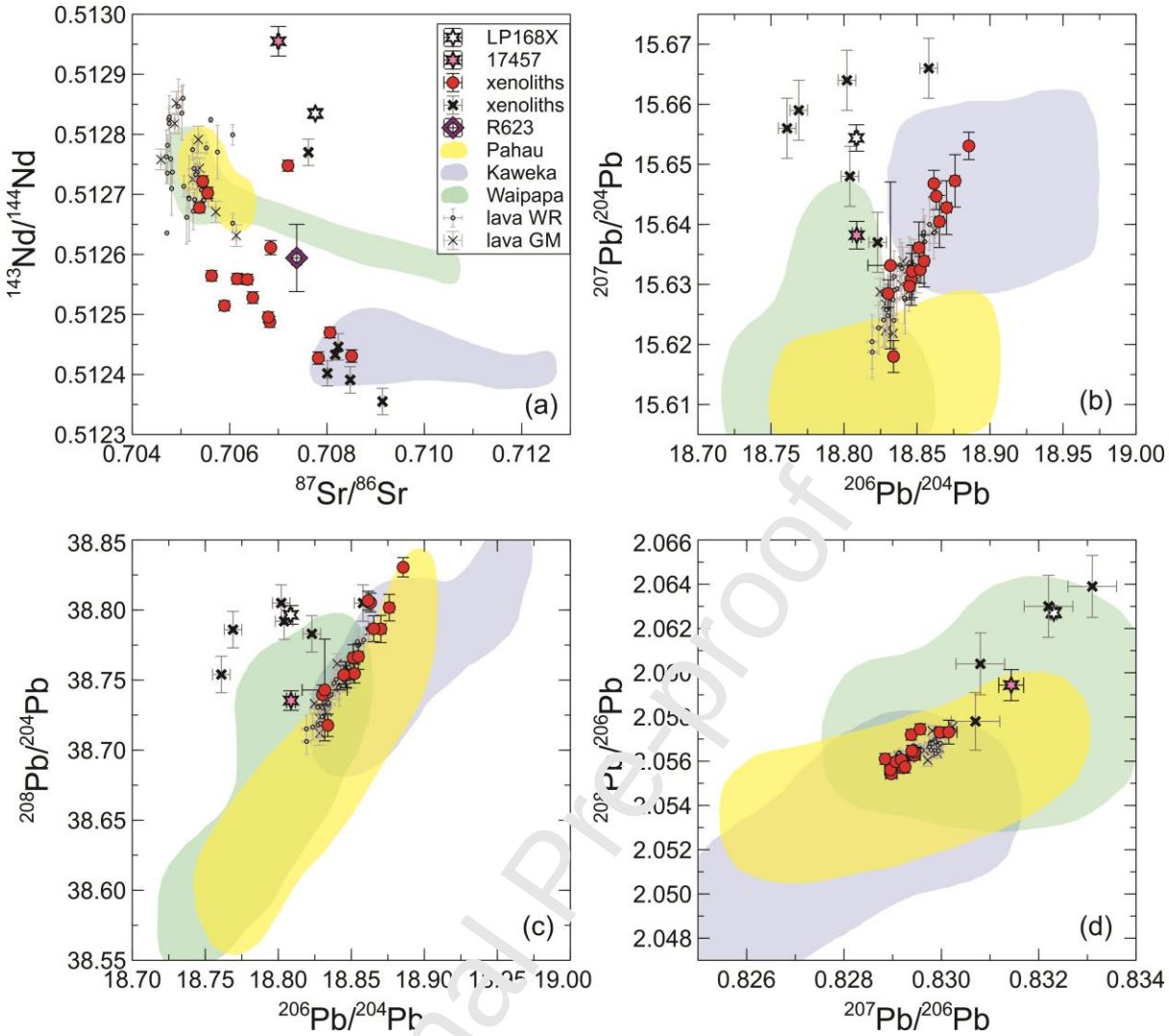


Fig. 7. Sr-Nd-Pb isotope ratios for xenoliths from Tongariro. Xenolith data are from this study (red filled circles) and Price et al. (2010: black crosses; all from the 1975 Ngāuruhoe pyroclastic flow deposits). Other xenolith data are from Rabbish Tip Dome (R623: Sutton, 1995) and Ruapehu volcano (17457: Graham, 1995; Lee, 2008). Whole-rock (WR) lava data are from Hobden (1997) and Pure (2020). Tongariro groundmass (GM) data are from Pure (2020). Data are plotted with 2 s.d. errors. Errors are included in the Pahau, Kaweka and Waipapa terrane fields: data from Price et al. (2015). Full xenolith data are contained in Table 3.

4. DISCUSSION

4.1. Xenolith source lithologies

Petrographic, chemical and isotopic features of basement xenoliths at Tongariro indicate they were sourced from metasedimentary rocks. Common feldspar and/or quartz in xenoliths suggest a felsic protolith, whereas rare zoisite favours a metasedimentary protolith, as opposed to igneous (Table 1). Xenoliths typically display LREE enrichment relative to HREEs which also

303 supports a felsic, continental crustal protolith (Fig. 6). Sr isotopic compositions of all xenoliths
304 exceed $^{87}Sr/^{86}Sr = 0.7050$ (Table 3), which is above the highest value (0.70359) reported for
305 oceanic basalts from the Havre Trough (Fig. 1), or $^{87}Sr/^{86}Sr = 0.70391$ in the relevant sample
306 after an additional 200 Myr of radiogenic ingrowth (Gill et al., 2020). Nd isotopic compositions
307 also indicate that xenoliths are not derived from oceanic crust. The highest $^{143}Nd/^{144}Nd$ ratio
308 recorded in a Tongariro xenolith is 0.51284 (LP168X: Table 3) which restores to an initial
309 $^{143}Nd/^{144}Nd$ of 0.51261, assuming an age of 200 Ma. This value is more similar to reference
310 sediments (e.g. Price et al., 2015) than $^{143}Nd/^{144}Nd$ ratios in <2 Ma basalts from the continental
311 TVZ (>0.5128; Gamble et al., 1993) and the oceanic (back-arc) Havre Trough (>0.5130: Gill et
312 al., 2020). This indicates that Tongariro basement xenoliths are derived from felsic continental
313 crust. Sample LP168X is also fine-grained and cut by a vein that likely comprises
314 metamorphosed quartz and calcite (see discussion below and Graham et al., 1988), which favour
315 a metasedimentary protolith over a plutonic protolith. Furthermore, petrographic, chemical and
316 isotopic data provide no strong evidence to suggest that any xenoliths in Tongariro or Ruapehu
317 eruptives were derived from a non-metasedimentary basement lithology (cf. Graham et al.,
318 1990). Arguments for a meta-igneous oceanic crust lithology in sub-Ruapehu basement rocks are
319 discussed below.
320
321 **4.2. Mineralogy of upper crustal basement rocks and xenoliths**
322 The mineral assemblages of upper crustal rocks beneath Tongariro are unknown from
323 direct observations. However, drill core samples of Kaweka and Waipapa terrane greywackes,
324 from east and west of Tongariro, respectively, contain feldspar, quartz, biotite, epidote, white
325 mica, pumpellyite, stilpnomelane, chlorite, Fe-Ti-Ca oxides, calcite and prehnite, plus lithic
326 fragments of granite, volcanic rocks and chert (Beetham and Watters, 1985). Similar mineral
327 assemblages probably occur in the basement rocks immediately beneath Tongariro because
328 exhumed Kaweka and Waipapa terrane rocks did not exceed greenschist facies temperature-

Journal Pre-proof

329 pressure conditions. Most samples reported by Jiao et al. (2014) remained within zeolite and
330 prehnite-pumpellyite facies conditions, as also reported by Beetham and Watters (1985) for
331 Kaweka terrane rocks. Similar mineral assemblages are also reported in exhumed South Island
332 metasedimentary schists (Grapes and Watanabe, 1994; Scanlan et al., 2020), which have similar
333 bulk compositions to low-grade Kaweka and Waipapa terrane rocks in the North Island (Grapes
334 et al., 1982; Price et al., 2015). Other drillhole samples of Kaweka and Waipapa terrane rocks,
335 from 100 to 200 km north of Tongariro, also contain white mica, illite, chlorite, quartz, feldspar,
336 epidote, calcite and andalusite, despite being hydrothermally altered (Milicich et al., 2021). Such
337 assemblages are anticipated to be common in the country rocks enveloping andesitic magma
338 bodies and conduits beneath Tongariro.

339 The absence of white mica, illite, chlorite, prehnite-pumpellyite, calcite, andalusite and
340 stilpnomelane in Tongariro xenoliths described here, and the minor amounts of biotite, strongly
341 suggest that country rock fragments underwent substantial mineralogical changes when they
342 were pyrometamorphosed after being entrained by magmas, which was likely associated with
343 chemical and isotopic changes (Figs. 5, 6a, 7, 8). This interpretation is supported by the presence
344 of tourmaline, corundum, sillimanite and pockets of brown glass in xenoliths, which are not
345 reported in samples of Kaweka and Waipapa terrane rocks (cf. Beetham and Watters, 1985;
346 Graham, 1987; Price et al., 2015; Milicich et al., 2021). Furthermore, the pockets of brown glass
347 (quenched melt) that occur along crystal boundaries (Fig. 3c) provide textural evidence for partial
348 melting, as described by Holness and Siklos (2000) and Holness et al. (2011). Many of the
349 minerals absent in xenoliths, such as white mica, chlorite, illite, quartz and epidote (except for
350 zoisite in rare cases: Table 1), likely melted or dissolved when the metasedimentary basement
351 rocks were stoped from wall rocks and channels where andesite magmas ascended. What is
352 unclear, however, is the level of textural and compositional heterogeneity that existed on mm-
353 scales in protoliths. Potentially, the micaceous domains in protoliths may have occurred in
354 millimetre to centimetre sized bands that are not represented by the surviving xenoliths.

Nonetheless, the dearth of white mica, chlorite, illite, quartz and epidote in Tongariro xenoliths, despite their abundance in Kaweka and Waipapa terrane drill core samples regionally (Beetham and Watters, 1985; Milicich et al., 2021), suggests partial melting and loss of up to 50% of the protolith.

Some of the minerals present in xenoliths, such as quartz, zircon, tourmaline, corundum, zoisite and biotite, do not occur as phenocryst phases in Tongariro andesite magmas (Table 1; Fig. 3). However, plagioclase, pyroxene and Fe-Ti oxides are abundant both in xenoliths and as phenocryst phases in the host andesites, which suggests that the mineral assemblages of xenoliths largely re-equilibrated to andesite magmatic temperatures, as previously suggested by Graham (1987). Experimental phase relations indicate that xenoliths experienced temperatures of >800 °C, at depths possibly shallower than 5 km, in eruptives from Ngāuruhoe (Graham et al., 1988). Two-pyroxene and titanomagnetite-ilmenite geothermometry indicates that xenoliths in Tongariro and Ruapehu eruptives experienced temperatures between ~800 and 980 °C (Graham, 1987; Graham et al., 1990). These approach typical temperatures of ~800 to 1000 °C estimated for Tongariro eruptives by Hobden (1997) and are much higher than typical greenschist facies temperatures where minerals such as white mica, chlorite and epidote are stable.

At andesitic magmatic temperatures, the breakdown products of white mica + quartz are mullite (or corundum) + sanidine (or potassic peraluminous melt), which occurs via dehydroxylation at ≤750 °C (e.g. Guggenheim et al., 1987; Rodriguez-Navarro et al. 2003). The presence of mullite in Ruapehu metasedimentary xenoliths (Graham, 1985) and corundum in Tongariro xenoliths (Table 1) supports this interpretation, as are the lower K_2O concentrations in xenoliths (0-1.5 wt%), relative to their likely protoliths (1-4 wt%) (Price et al., 2015; Conway et al., 2018). The varied proportions of spinel, orthopyroxene, cordierite, magnetite and biotite in Tongariro and Ruapehu xenoliths provide further evidence that country rock assimilation

induced changes in xenolith mineralogy, because these minerals are produced from the pyrometamorphic breakdown of chlorite (Graham, 1987; Worden et al., 1987) (Table 1).

The lower SiO_2 concentrations in most xenoliths relative to the basement reference samples suggest a net loss of SiO_2-rich materials (Fig. 4). Even though removing white mica, illite, chlorite, epidote, prehnite and pumpellyite (~30-50 wt%) would increase xenolith SiO_2 concentrations, the opposite is observed wherein SiO_2 concentrations in xenoliths are lower than in their likely protoliths (Price et al., 2015; Scanlan et al., 2020). It is therefore likely that quartz dissolved in subequal proportions to the combined amount of low-SiO_2 minerals just mentioned. The scarcity of quartz, except where it forms >90% of xenoliths, implies that it dissolves in cotectic or eutectic reactions when it occurs in subequal amounts with other minerals (cf. Fig. 3a). The presence of high-SiO_2 basement rocks (i.e. >65 wt%) is demonstrated by quartz-rich xenoliths in Tongariro eruptives. Of such xenoliths, those comprising quartz, wollastonite and calcic plagioclase have been interpreted as quartz-calcite veins (Graham et al., 1988) that have elevated $^{87}Sr/^{86}Sr$ ratios (0.70757 to 0.70817) and 10-100s of ppm of trace elements (e.g. Price et al., 2010). In contrast, however, one pure-quartz xenolith analysed here (LP063X) has trace element concentrations within error of 0 ppm except for Li, B, Ti, Cu and Ba (all <15 ppm), which indicates a quartz-rich protolith. Based on Kaweka terrane drill core samples from east of Tongariro (Leetham and Watters, 1985), such quartz-rich xenoliths potentially represent chert beds or quartz veins whereas quartz-pyroxene-plagioclase xenoliths are more likely to represent metamorphosed quartz-calcite veins.

Unidentified minerals that form the yellow and white vein in LP168X are probably the replacement products of impure quartz and calcite veins because the thermal decomposition of quartz + calcite produces wollastonite + CO_2 (Harker and Tuttle, 1956). Under certain redox conditions, wollastonite and CO_2 could be represented by the hedenbergite, graphite and other minerals if some C is retained as graphite and if impurities in the quartz-calcite vein provides Fe, Mg and Al to form calcic pyroxenes other than wollastonite. This is supported by the quartz-

406 wollastonite-calcic plagioclase veins reported in Tongariro xenoliths by Graham et al. (1988) that
407 were also interpreted to be metamorphosed quartz-calcite veins. Potentially, the yellow and white
408 vein materials in LP168X comprise microfibres of wollastonite, other pyroxenes, calcic
409 plagioclase and silicic glasses that formed when the xenolith was pyrometamorphosed. Xenolith
410 17457 from Ruapehu, which shares the same unusual chemical and isotopic features (Figs. 4 to
411 7), is described as a vesicular "grey, fine-grained, inhomogeneous spinel-rich schist" (Graham,
412 1985), which broadly matches the description of LP168X (Table 1; Figs. 2d, 3d).
413
414 **4.3. Chemical and isotopic differences between xenoliths and reference samples**
415 The concentrations of K and other elements with similar chemical properties (e.g. Rb,
416 Ba, Cs) are lower in all xenoliths than in the basement reference samples (e.g. Figs. 4g, 5a, b, c),
417 as are the concentrations of radiogenic ^{87}Sr (Fig. 8a). These differences are attributed to
418 breakdown of the abundant white mica ± illite in xenoliths, and the incorporation of resulting
419 partial melts into the surrounding magma. The net effect of these mineralogical changes has
420 decreased $^{87}Sr/^{86}Sr$ ratios in xenoliths by ≥0.003 relative to their likely protoliths (Fig. 8a). A
421 difference of up 0.003 is indicated by basement reference samples that have $^{87}Sr/^{86}Sr$ ratios that
422 extend to ~0.712 (Price et al., 2015) whereas xenolith ratios are restricted to <~0.709, even
423 though $^{143}Nd/^{144}Nd$ ratios range from 0.5124 to 0.5128 for most xenoliths and reference
424 samples. Simple calculations show that a protolith with the average Kaweka terrane composition
425 (295 ppm Sr; 118 ppm Rb; $^{87}Sr/^{86}Sr$ = 0.709539: Price et al., 2015) will have an initial
426 $^{87}Sr/^{86}Sr$ ratio of 0.706477 if back-calculated from a 190 Ma age, which is supported by
427 $^{87}Sr/^{86}Sr$ ratios and ages reported by Adams et al. (2009). If the protolith loses 50% of its mass
428 during partial melting, the resulting melt will have 93 ppm Sr, 219 ppm Rb and $^{87}Sr/^{86}Sr$ =
429 0.706477 initially or $^{87}Sr/^{86}Sr$ = 0.723254 after 190 Myr, as estimated by mass balance against the
430 average xenolith's Rb (17 ppm) and Sr (497 ppm) concentrations (Table 2). Such high Rb
431 concentrations in melts are supported by melt inclusions with ~270 ppm Rb in a partially melted

metasedimentary xenolith from Ruapehu (Conway et al., 2018). Back-mixing 50% of the melt with 50% of the average xenolith predicts an average xenolith $^{87}Sr/^{86}Sr$ of 0.706966, which compares with the measured average xenolith $^{87}Sr/^{86}Sr$ of 0.706669 (Table 3). Depending on which xenolith $^{87}Sr/^{86}Sr$ ratio is chosen, there is a 0.0026 to 0.0029 difference between protolith and xenolith $^{87}Sr/^{86}Sr$ ratios, hence supporting the ≤0.003 offset.

Sm/Nd and $^{143}Nd/^{144}Nd$ ratios for xenoliths and reference samples are comparable (Fig. 8b), indicating that the xenoliths underwent little or no Sm/Nd fractionation after they were entrained in magmas. Only samples LP168X and 17457 show small amounts of Sm/Nd fractionation, which may explain their relatively higher $^{143}Nd/^{144}Nd$ ratios of 0.51284 to 0.51296. On this basis, the $^{143}Nd/^{144}Nd$ ratios of the other xenoliths should provide a reliable guide to their source terrane (provenance), using comparisons with the reference data for the different basement terranes (Price et al., 2015).

Pb isotope ratios cannot distinguish which terranes the xenoliths were likely derived from. Although $^{206}Pb/^{204}Pb$ and $^{208}Pb/^{204}Pb$ ratios support derivation from the Kaweka terrane, $^{208}Pb/^{206}Pb$ ratios are more similar to the Waipapa or Pahau terranes. Furthermore, $^{207}Pb/^{204}Pb$ and $^{207}Pb/^{206}Pb$ ratios imply that xenoliths were potentially derived from either of these terranes (Fig. 8c, d). These contradictory results are taken to indicate that some Pb isotope ratios in xenoliths may have been modified. Despite this, it is unclear how mineral proportions (modified by pyrometamorphism) are related to Pb isotopic compositions in xenoliths. We found no significant relationships between Pb isotopic ratios and the concentrations of Pb, Th and U or ratios of these elements (e.g. Fig. 8). Therefore, although mineral/melt partitioning coefficients of Pb, Th and U may be coupled with some Pb isotopic variation, we cannot deduce which minerals were the primary hosts of Pb, Th and U on present data.

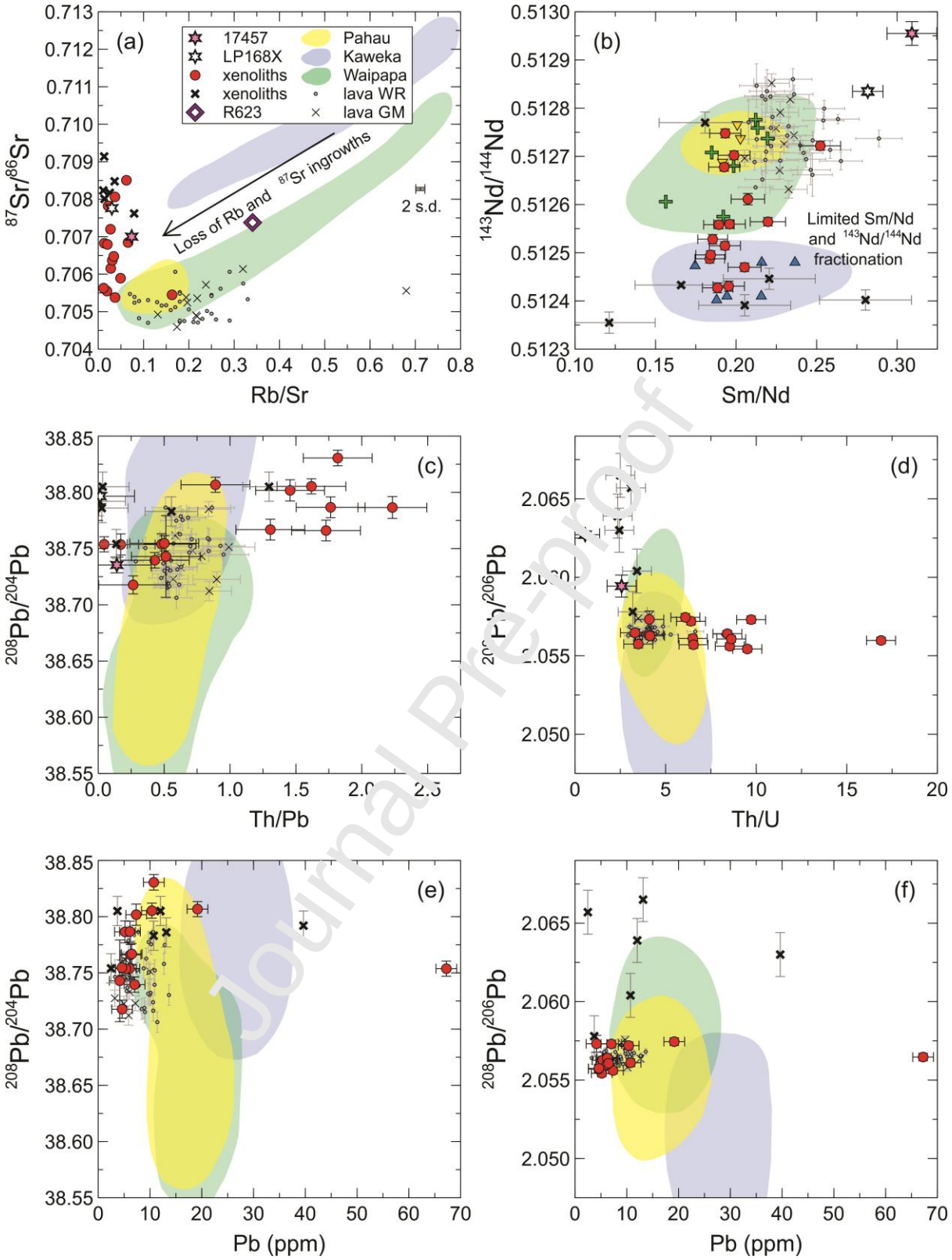


Fig. 8. Sr-Nd-Pb isotope ratios against their respective parent/daughter element ratios. **(a)** Rb/Sr versus $^{87}Sr/^{86}Sr$. **(b)** Sm/Nd versus $^{143}Nd/^{144}Nd$. **(c)** Th/Pb versus $^{208}Pb/^{204}Pb$. **(d)** Th/U versus $^{208}Pb/^{206}Pb$. **(e)** Pb versus $^{208}Pb/^{204}Pb$. **(f)** Pb versus $^{208}Pb/^{206}Pb$. Xenolith data are from this study (red filled circles) and Price et al. (2010: black crosses; all from the 1975 Ngāuruhoe pyroclastic flow deposits). Other xenolith data are from Rubbish Tip Dome at Taupō volcano (sample R623: Sutton, 1995) and Ruapehu volcano (sample 17457: Graham, 1995; Lee, 2008). Whole-rock (WR) lava data are from Hobden (1997)

and Pure (2020). Tongariro groundmass (GM) data are from Pure (2020). Data are plotted with 2 s.d. errors. Errors are included in the Pahau, Kaweka and Waipapa terrane fields: data from Price et al. (2015).

4.4. Heterogeneities in basement rocks: the 'nugget effect'

Most xenoliths analysed in this study are <10 g in total mass and may be unrepresentative of their bulk protoliths (Table 1). Millimetre-scale heterogeneities in the textures and compositions of protoliths may be over-represented in some xenoliths that contain minerals that are stable at andesitic magma temperatures, i.e. the 'nugget effect'. The selective preservation of some minerals during pyrometamorphism will facilitate the preferential loss of certain elements (and isotopes) whilst retaining others. This phenomenon may explain some of the compositional differences between xenoliths and basement reference samples, which is considered for the two largest xenoliths: LP134X (11.2 g) and LP215X (13.0 g) (Table 1).

LP134X is the only xenolith reported here with similar SiO_2 to basement reference samples (63 wt%: Fig. 3). This xenolith also closely overlaps with the REE field for the Waipapa and Pahau terranes (Fig. 6a) and possesses Sr and Nd isotopic compositions most similar to the Waipapa terrane (Fig. 7a; Table 3). Conversely, LP215X has chemical and isotopic features that support both Kaweka and Waipapa terrane protoliths (Figs. 6a, 7a, Table 3). Notably, despite being smaller than LP215X, five other xenoliths weighing 0.6 to 8.6 g have even higher $^{87}Sr/^{86}Sr$ and even lower $^{143}Nd/^{144}Nd$ ratios, which indicate Kaweka terrane provenance (Tables 1, 3; Fig. 7a). Textural and composition heterogeneities occurring on mm-scales in protoliths are therefore expressed variably in surviving xenoliths, and that larger xenoliths may more accurately reflect their protolithic compositions. Hence, chemical and isotopic data for LP134X and LP215X indicate Tongariro xenoliths were derived from both Waipapa and Kaweka terranes.

4.5. Terrane provenance of xenoliths

Notwithstanding the potential over-representation of mm-scale compositional heterogeneities in their protoliths, Nd isotope ratios are the best available tool for inferring the

490 provenance of the Tongariro xenoliths because Sr and Pb isotope ratios and most absolute
491 element concentrations of xenoliths differ from their likely protoliths (Fig. 8). The basement
492 reference samples reported by Price et al. (2015) show that Kaweka terrane rocks possess
493 $^{143}Nd/^{144}Nd$ ratios ≤0.5125, which is a feature shared with 10 of the combined 21 xenoliths
494 reported here (Table 3) and by Price et al. (2010) with known Sr-Nd-Pb isotopic compositions,
495 but excluding LP168X (see below). The 11 other xenoliths have $^{143}Nd/^{144}Nd$ ratios >0.5125
496 which suggests that Kaweka and non-Kaweka terrane basement rocks exist beneath Tongariro.
497 The most likely non-Kaweka metasedimentary rocks to occur beneath Tongariro are from the
498 Waipapa terrane which crops out immediately west of Tongariro (Fig. 1) (Beetham and Watters,
499 1985; Jiao et al., 2014; Price et al., 2015; Townsend et al., 2017; Milicich et al., 2021).
500 The compositions of LP168X and 17457 (from Ruapehu) differ from other Tongariro
501 basement xenoliths reported here and by Price et al. (2010) in their higher Nd isotope ratios
502 (0.51284-0.51296), negative Ce anomalies and flatter REE curves (La_N/Yb_N ~2). These chemical
503 differences are inferred to be related to the presence of pyrometamorphosed quartz-calcite veins
504 in these xenoliths or the localised effects of CO_2 (from calcite breakdown) on REE-hosting
505 minerals. LP168X is demonstrably metasedimentary in origin because of its mineralogy (Table 1)
506 and its similarity to other metasedimentary xenoliths reported here and by Graham et al. (1988);
507 xenolith 17457 was also classified as metasedimentary by Graham (1985). Neither LP168X nor
508 17457 are likely to be cognate xenoliths associated with Quaternary volcanism because both have
509 $^{87}Sr/^{86}Sr$ ratios >0.707, whereas $^{87}Sr/^{86}Sr$ ratios in eruptives from Tongariro and Ruapehu rarely
510 exceed 0.706 (Hobden, 1997; Price et al., 2012; Pure, 2020) (Fig. 7a). In contrast with Graham et
511 al. (1990), we conclude that above-average $^{143}Nd/^{144}Nd$ ratios and MgO concentrations in these
512 xenoliths do not require derivation from basement basaltic oceanic crust.
513
514
515

Journal Pre-proof

Journal Pre-proof

516 **4.6. Xenolith mass loss and restite production**

517 We estimated the mass losses from Tongariro xenoliths using isocon analysis, following
518 Gresens (1967) and Grant (1981). Isocons, or lines of unchanged chemical mass, are best-fit lines
519 defined by immobile elements that are inferred to have been neither lost nor added during
520 alteration/recystallisation, relative to their original masses in the protolith. For a single mass loss
521 event when country rock fragments are assimilated, pyrometamorphosed and partially melted,
522 bulk element concentrations and masses are related by $C_A = C_0(M_0/M_A)$, where C_A is the altered
523 concentration (xenolith), C_0 is the initial concentration (protolith). M_0 is the initial mass
524 (protolith before assimilation) and M_A is the altered mass (final mass of restitic xenolith). The
525 gradient of the isocon (C_A/C_0), defined by immobile elements, is directly related to the fraction
526 of mass loss (M_A/M_0) by $M_A/M_0 = 1/(C_A/C_0)$.

527

Journal Pre-proof

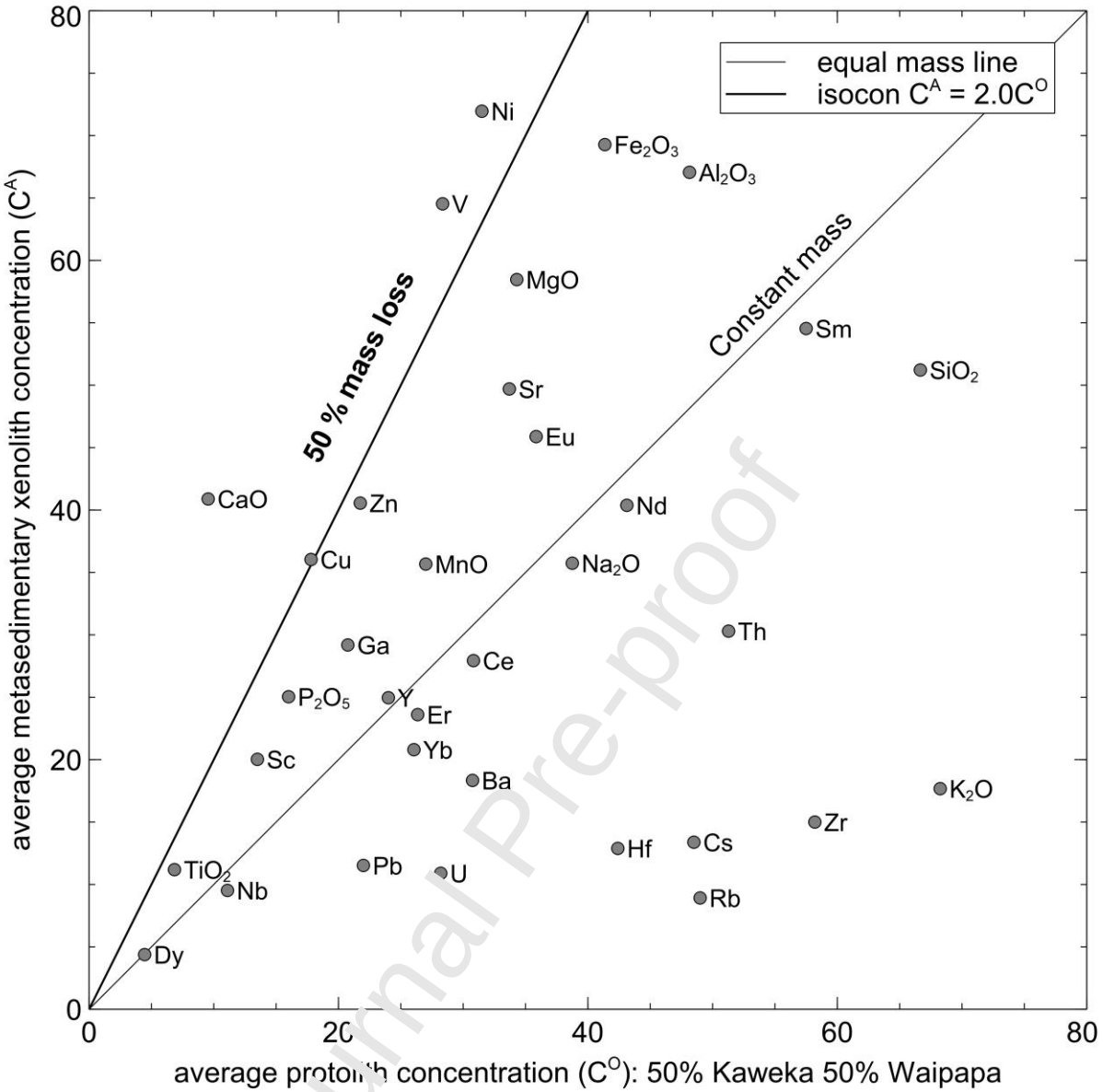


Fig. 9. Isocon diagram for the average basement xenolith composition against an average basement metasediment composition. The average xenolith composition only uses data from this study to avoid bias towards the Holocene record in Price et al. (2010). The average basement composition is estimated as 50% Kaweka terrane and 50% Waipapa terrane, using the average compositions recommended by Price et al. (2015), following the discussion in section 4.5. The bold line plots through immobile elements that underwent the least mass loss (and were retained in xenoliths); a constant mass line is also shown. Most elements contained in feldspars, pyroxene and major elements in Fe-Ti oxides plot around the 50% mass loss isocon. All compositional data, originally in wt% or ppm, are scaled by the factors (given in supplementary materials) to improve visual clarity in the plot, following Grant (1981).

In the average Tongariro xenolith, the most immobile elements and oxides (TiO_2, Al_2O_3, Fe_2O_3, MnO, MgO, CaO, P_2O_5, Ni, V, Cu, Zn, Sr, Ga, Sc, Eu) define an isocon with $C_A/C_0 = 2$, that is, a ~50% mass loss (Fig. 9). This estimate assumes a protolith composition comprising

542 50% Kaweka terrane and 50% Waipapa terrane, using the average compositions suggested by
543 Price et al. (2015) and xenolith provenance interpretations given above (the isocon result
544 obtained when using pure a Kaweka or Waipapa terrane average composition is also a ~50%
545 mass loss). The immobile elements mentioned above are commonly contained in plagioclase,
546 pyroxene, corundum, Fe-Ti oxides, biotite, apatite and spinel (e.g. Rollinson, 1993), which occur
547 in Tongariro xenoliths (Table 1; Fig. 3). The most mobile elements and oxides (K, Rb, Cs, Ba,
548 Pb, Th, U, Hf, Zr), which were largely removed from xenoliths (Figs. 4g, 5c, e, f), are commonly
549 hosted in white mica, illite, zircon and minerals containing high field strength elements.
550 Depletions in SiO_2 also indicate substantial loss of quartz, as discussed in section 4.2 The ~50%
551 mass loss estimated for Tongariro basement xenoliths is similar to a 30-55% mass loss reported
552 for greenschist facies metapelites that were incorporated in dacite magmas at El Joyazo volcano,
553 Spain, which was estimated from the compositions of xenoliths, lava groundmasses, xenolith-
554 hosted glasses and reference metapelites (Cesare et al., 1997). Similarly, mass balance modelling
555 indicates that gneissic xenoliths (of inferred metasedimentary origin) underwent mass losses of
556 60% when they were incorporated into mafic intrusive rocks in Voisey's Bay Intrusion, Canada
557 (Mariga et al., 2006), which also supports the isocon analysis results for xenoliths at Tongariro.
558
559 **4.7. Assimilation: bulk or partial protolith incorporation?**
560 Micro-scale investigations on natural and experimental materials indicate that magma-
561 country rock interactions typically cause partial rather than wholesale melting of country rock
562 (e.g. Knesel and Davidson, 1996, 1999; Tommasini and Davies, 1997). These processes have
563 been modelled numerically (Zeng et al., 2005; Farina and Stevens, 2011) and demonstrated by
564 outcrop-scale studies of plutonic rocks (White and Chappell, 1977; Petcovic and Grunder, 2003;
565 Farina et al., 2014; Wolf et al., 2019). Here we consider whether assimilant compositions are
566 more closely represented by partial melts derived from country rock (with contrasting
567 compositions to the bulk protolith) or the country rock bulk composition itself.

Journal Pre-proof

In the first case, partial melts may be derived from wall rocks without incorporating associated restites and will have contrasting compositions to their protoliths (Knesel and Davidson, 1996, 1999). In the second case, partial fusion of country rock may facilitate stoping by reducing the cohesion between internal grain boundaries in wall rock material and encouraging shearing and fragmentation induced by magma flow, resulting in the combined incorporation of partial melts and restites with the same net composition as the protolith (e.g. White and Chappell, 1977). In Tongariro andesites, the survival of refractory country rock xenoliths that re-equilibrated at magmatic temperatures suggests that the dominant assimilation process involves the combined incorporation of both partial melts and restites (Graham, 1987; Graham et al., 1988). When both components are assimilated, the heat costs of crystallisation may not counterbalance the heat costs of country rock fusion because assimilation proceeds without the complete melting of country rock. Put differently, the mass of assimilation/mass of crystallisation ratio (the r-value of DePaolo, 1981) may exceed 1 without violating thermodynamics because only a fraction of the assimilant need be melted for it to be mechanically and chemically incorporated in full. Despite opposition to this hypothesis (Glazner and Bartley, 2006; Glazner, 2007), it is likely that country rock stoping is a common process in generation of arc magmas (White and Chappell, 1977; Paterson et al., 2008). For the purposes of modelling bulk chemical arrays, the original AFC formulation by DePaolo (1981) should accurately reflect chemical evolution pathways because net assimilant compositions are effectively the same as bulk country rock compositions. However, we emphasise that r-values are not restricted to values of <1, as in the original DePaolo (1981) formulation, because assimilation and crystallisation are not always thermodynamically balanced processes (e.g. Sisson et al., 2014).

Journal Pre-proof

Journal Pre-proof

5. CONCLUSIONS

Metasedimentary xenoliths erupted in Tongariro andesites are restites that were derived from basement rocks comprising the Kaweka and Waipapa terranes. Previous suggestions that some xenoliths represent fragments of meta-igneous oceanic crust are not supported by chemical and isotopic data. In general, xenolith compositions differ from potential metasedimentary protoliths (the Kaweka, Waipapa and Pahau terranes). These compositional differences are jointly explained by selective partial melting and dissolution of certain minerals—notably white mica, illite, chlorite, epidote and quartz—and mm-scale compositional heterogeneities in protoliths that may be over-represented in small (<10 g) xenoliths. Partial melting and dissolution of the minerals just mentioned occurred when xenoliths were entrained in andesite magmas at ~800 to 1000 °C (Graham, 1987; Hobden, 1997). Surviving mineral assemblages contain plagioclase, alkali feldspar, pyroxene, Fe-Ti oxides, quartz, apatite, biotite, glass, zircon, zoisite, tourmaline, corundum and spinels. Mineral changes in xenoliths were accompanied by mass losses of ~50%, which is reflected in the lower concentrations of SiO_2, K_2O, Rb, Ba, Cs, Zr, Hf, U, Pb, Th and some REEs (but not Eu), and lower $^{87}Sr/^{86}Sr$ values, relative to their protoliths. Nd isotope ratios, however, appear to be relatively unaffected by pyrometamorphic changes and may reliably indicate the provenance of most xenoliths. On the basis of $^{143}Nd/^{144}Nd$ ratios, 10 xenoliths are associated with the Kaweka terrane and 11 others with the Waipapa terrane. In addition to these 21 xenoliths, another xenolith with high $^{143}Nd/^{144}Nd$ (0.51284), a negative Ce anomaly and low La_N/Yb_N (~2) contains quartz-calcite veins that reacted to form hedenbergite, pigeonite, augite, wollastonite, calcic plagioclase, silicic glass and graphite.

ACKNOWLEDGEMENTS

LRP was supported by a PhD Scholarship from Victoria University of Wellington, with additional support from the ECLIPSE Programme funded by the New Zealand Ministry of Business, Innovation and Employment and GNS Science. We thank the Ngati Tūwharetoa iwi

620 (through the Department of Conservation and GNS Science) for permission to undertake
621 scientific sampling and Bubs Smith for his support of this work. Analytical costs were supported
622 by the Earthquake Commission of New Zealand grant 16/U735. We thank Andrew Galloway
623 and Kerstin Gruender for assistance with laboratory work. Anita Grunder, Jim Cole, Kevin
624 Norton, Roger Briggs, Nick Mortimer and an anonymous reviewer are thanked for their
625 constructive comments which improved this manuscript.

626

Journal Pre-proof

REFERENCES

Adams, C.J., Mortimer, N., Campbell, H.J., Griffin, W.L., 2009. Age and isotopic characterisation of metasedimentary rocks from the Torlesse Supergroup and Waipapa Group in the central North Island, New Zealand, N.Z. J. Geol. Geophys. 52, 149-170.

Beavan, J., Wallace, L.M., Palmer, N., Denys, P., Ellis, S., Fournier, N., Hreinsdottir, S., Pearson, C., Denham, M., 2016. New Zealand GPS velocity field: 1995–2013. N.Z. J. Geol. Geophys. 59, 5-14.

Beetham, R.D., Watters, W.A., 1985. Geology of Torlesse and Waipapa terrane basement rocks encountered during the Tongariro Power Development project, North Island, New Zealand. N.Z. J. Geol. Geophys. 28, 575-594.

Behr, Y., Townend, J., Bannister, S., Savage, M.K., 2011 Crustal shear wave tomography of the Taupo Volcanic Zone, New Zealand, via ambient noise correlation between multiple three-component networks. Geochem. Geophys. Geosyst. 12, Q03015.

Cesare, B., Mariani, E.S., Venturelli, G., 1997. Crustal anatexis and melt extraction during deformation in the restitic xenoliths at El Joyazo (SE Spain). Min. Mag. 61, 15-27.

Charlier, B.L.A., Ginibre, C., Morgan, D., Nowell, G.M., Pearson, D.G., Davidson, J.P., Ottley, C.J., 2006. Methods for the microsampling and high-precision analysis of strontium and rubidium isotopes at single-crystal scale for petrological and geochronological applications. Chem. Geol. 232, 114-133.

Charlier, B.L.A., Wilson, C.J.N., Mortimer, N., 2010. Evidence from zircon U-Pb age spectra for crustal structure and felsic magma genesis at Taupo volcano, New Zealand. Geology 38, 915-918.

Conway, C.E., Gamble, J.A., Wilson, C.J.N., Leonard, G.S., Townsend, D.B., Calvert, A.T., 2018. New petrological, geochemical, and geochronological perspectives on andesite-dacite magma genesis at Ruapehu volcano, New Zealand. Am. Mineral. 103, 565-581.

Cronin, S.J., Neall, V.E., 1997. A late Quaternary stratigraphic framework for the northeastern Ruapehu and eastern Tongariro ring plains, New Zealand. N.Z. J. Geol. Geophys. 40, 185-197.

DePaolo, D.J., 1981. Trace element and isotopic effects of combined wallrock assimilation and fractional crystallization. Earth Planet. Sci. Lett. 53, 189-202.

Farina, F., Stevens, G., 2011. Source controlled $^{87}Sr/^{86}Sr$ isotope variability in granitic magmas: the inevitable consequence of mineral-scale isotopic disequilibrium in the protolith. Lithos 122, 189-200.

Farina, F., Dini, A., Rocchi, S., Stevens, G., 2014. Extreme mineral-scale Sr isotope heterogeneity in granites by disequilibrium melting of the crust. Earth Planet. Sci. Lett. 399, 103-115.

Gamble, J.A., Smith, I.E.M., McCulloch, M.T., Graham, I.J. and Kokelaar, B.P., 1993. The geochemistry and petrogenesis of basalts from the Taupo Volcanic Zone and Kermadec Island Arc, S.W. Pacific. J. Volcanol. Geotherm. Res. 54, 265-290.

Gill, J., 1981. Orogenic Andesites and Plate Tectonics. Springer-Verlag, New York, 390 pp.

Gill, J., Hoernle, K., Todd, E., Hauff, F., Werner, R., Timm, C., Garbe-Schönberg, D., Gutjahr, M., 2020. Basalt geochemistry and mantle flow during early backarc basin evolution: Havre Trough and Kermadec Arc, southwest Pacific. Geochem. Geophys. Geosyst. 22, e2020GC009339.

Journal Pre-proof

Glazner, A.F., 2007. Thermal limitations on incorporation of wall rock into magma. Geology 35, 319-322.

Glazner, A.F., Bartley, J.M., 2006. Is stoping a volumetrically significant pluton emplacement process? Geol. Soc. Am. Bull. 118, 1185-1195.

Gómez-Vasconcelos, M.G., Villamor, P., Cronin, S., Proctor, J., Palmer, J., Townsend, D., Leonard, G., 2017. Crustal evolution in the Tongariro graben, New Zealand: Insights into volcano-tectonic interactions and active deformation in a young continental rift. Geol. Soc. Am. Bull. 129, 1085-1099.

Graham, I.J., 1985. Petrochemical and Sr-isotopic studies of lavas and xenoliths from Tongariro Volcanic Centre: implications for crustal contamination of calc-alkaline magmas. Unpublished PhD thesis, Victoria University of Wellington, New Zealand, 345 pp.

Graham, I.J., 1987. Petrography and origin of metasedimentary xenoliths in lavas from Tongariro Volcanic Centre. N.Z. J. Geol. Geophys. 30, 139-157.

Graham, I.J., Hackett, W.R., 1987. Petrology of calc-alkaline lavas from Ruapehu volcano and related vents, Taupo Volcanic Zone, New Zealand. J. Petrol. 38, 531-567.

Graham, I.J., Grapes, R.H., Kifle, K., 1988. Buchitic metagreywacke xenoliths from Mount Ngauruhoe, Taupo Volcanic Zone, New Zealand. J. Volcanol. Geotherm. Res. 35, 205-216.

Graham, I.J., Blattner, P., McCulloch, M.T., 1990. Meta-igneous granulite xenoliths from Mount Ruapehu, New Zealand: fragments of altered oceanic crust? Contrib. Mineral. Petrol. 105, 650-661.

Grant, J.A., 1981. The isocon diagram—a simple solution to Gresens' equation for metasomatic alteration. Econ. Geol. 81, 1976-1982.

Grapes, R., Watanabe, T., 1994. Mineral composition variation in Alpine Schist, Southern Alps, New Zealand: Implications for recrystallisation and exhumation. Island Arc 3, 163-181.

Grapes, R., Watanabe, T., Palmer, K., 1992. XRF analyses of quartzo-feldspathic schists and metacherts, Franz Josef-Fox Glacier area, Southern Alps of New Zealand. Department of Geology, Victoria University of Wellington, Publication 25.

Gresens, R.L., 1967. Composition-volume relationships of metasomatism. Chem. Geol. 2, 47-55.

Guggenheim, S., Chang, Y.-H., Koster van Groos, A.F., 1987. Muscovite dehydroxylation: high-temperature studies. Am. Mineral. 72, 537-550.

Harker, R.I., Tuttle, O.F., 1956. Experimental data on the P(sub CO_2)-T curve for the reaction: calcite + quartz <-> wollastonite + carbon dioxide. Am. J. Sci. 254, 239-256.

Harrison, A., White, R.S., 2006. Lithospheric structure of an active backarc basin: the Taupo Volcanic Zone, New Zealand. Geophys. J. Int. 167, 968-990.

Hobden, B.J., 1997. Modelling magmatic trends in space and time: eruptive and magmatic history of the Tongariro volcanic complex. Unpublished PhD thesis, University of Canterbury, Christchurch, New Zealand, 508 pp.

Holness, M.B., Siklos, S.T.C., 2000. The rates and extent of textural equilibration in high-temperature fluid-bearing systems. Chem. Geol. 162, 137-153.

Holness, M.B., Cesare, B., Sawyer, E.W., 2011. Melted rocks under the microscope: microstructures and their interpretation. Elements 7, 247-252.

Jiao, R., Seward, D., Little, T.A., Kohn, B.P., 2014. Thermal history and exhumation of basement rocks from Mesozoic to Cenozoic subduction cycles, central North Island, New Zealand. Tectonics 33, 1920-1935.

Journal Pre-proof

Jochum, K.P., Weis, U., Schwagger, B., Stoll, B., Wilson, S.A., Haug, G.H., Andreae, M.O., Enzweiler, J., 2016. Reference values following ISO guidelines for frequently requested rock reference materials. Geostand. Geoanal. Res. 40, 333-350.

Knesel, K.M., Davidson, J.P., 1996. Isotopic disequilibrium during melting of granite and implications for crustal contamination of magmas. Geology 24, 243-246.

Knesel, K.M., Davidson, J.P., 1999. Sr isotope systematics during melt generation by intrusion of basalt into continental crust. Contrib. Mineral. Petrol. 136, 285-295.

Lee, T.R., 2008. The thermal evolution of subduction zone lithosphere: evidence from the chemical development of Mt. Ruapehu and surrounding vents, New Zealand. Unpublished PhD thesis, University of Durham, United Kingdom, 238 pp.

Lugmair, G.W., Carlson, R.W., 1978. The Sm-Nd history of KREEP. Proc. 9th Lunar Planet. Sci. Conf., Houston, Texas, 689-704.

Mariga, J., Ripley, E.M., Li, C., 2006. Petrologic evolution of gneissic xenoliths in the Voisey's Bay Intrusion, Labrador, Canada: Mineralogy, reactions, partial melting, and mechanisms of mass transfer. Geochem. Geophys. Geosyst. 7, Q05013.

McDonough, W.F., Sun, S.-s., 1995. The composition of the Earth. Chem. Geol. 120, 223-253.

Milicich, S.D., Mortimer, N., Villamor, P., Wilson, C.J.N., Chambefort, I., Sagar, M.W., Ireland, T.R., 2021. The Mesozoic terrane boundary beneath the Taupo Volcanic Zone, New Zealand, and potential controls on geothermal system characteristics. N.Z. J. Geol. Geophys. (in press, doi:10.1080/00288306.2020.1823434).

Mortimer, N., 1994. Origin of the Torlesse and coeval rocks, North Island, New Zealand. Int. Geol. Rev. 36, 891-910.

Mortimer, N., Rattenbury, M.S., King, P.R., Bland, K.J., Barrell, D.J.A., Bache, F., Begg, J.G., Campbell, H.J., Cox, S.C., Crampton, J.S., Edbrooke, S.W., Forsyth, P.J., Johnston, M.R., Jongens, R., Lee, J.M., Leonard, G.S., Raine, J.I., Skinner, D.N.B., Timm, C., Townsend, D.B., Tulloch, A.J., Turnbull, I.M., Turnbull, R.E., 2014. High-level stratigraphic scheme for New Zealand rocks. N.Z. J. Geol. Geophys. 57, 402-419.

Munoz, J.L., Ludington, S.D., 1974. Fluorine-hydroxyl exchange in biotite. Am. J. Sci. 274, 396-413.

Nicol, A., Mazengarb, C., Chanier, F., Rait, G., Uruski, C., Wallace, L. (2007). Tectonic evolution of the active Hikurangi subduction margin, New Zealand, since the Oligocene. Tectonics 26, TC4002.

Paterson, S.R., Pignotta, G.S., Farris, D., Memeti, V., Miller, R.B., Vernon, R.H., Žák, J., 2008. Is stoping a volumetrically significant pluton emplacement process?: Discussion. Geol. Soc. Am. Bull. 120, 1075-1079.

Petcovic, H.L., Grunder, A.L., 2003. Textural and thermal history of partial melting in tonalitic wallrock at the margin of a basaltic dike, Wallowa Mountains, Oregon. J. Petrol. 44, 2287-2312.

Pin, C., Gannoun, A., Dupont, A., 2014. Rapid, simultaneous separation of Sr, Pb and Nd by extraction chromatography prior to isotope ratios determination by TIMS and MC-ICP-MS. J. Anal. Atom. Spectrom. 29, 1858-1870.

Price, R.C., Turner, S., Cook, C., Hobden, B., Smith, I.E.M., Gamble, J.A., Handley, H., Maas, R., Möbis, A., 2010. Crustal and mantle influences and U-Th-Ra disequilibrium in andesitic lavas of Ngauruhoe volcano, New Zealand. Chem. Geol. 277, 355-373.

Journal Pre-proof

Price, R.C., Mortimer, N., Smith, I.E.M., Maas, R., 2015. Whole-rock geochemical reference data for Torlesse and Waipapa terranes, North Island, New Zealand. N.Z. J. Geol. Geophys. 58, 213-228.

Pure, L.R., 2020. The volcanic and magmatic evolution of Tongariro volcano, New Zealand. PhD thesis, Victoria University of Wellington, Wellington, New Zealand, 436 pp.

Pure, L.R., Townsend, D.B., Leonard, G.S., Wilson, C.J.N., Calvert, A.T., Cole, R.P., Conway, C.E., Gamble, J.A., Smith, T.B., 2020. A high resolution $^{40}Ar/^{39}Ar$ lava chronology and edifice construction history for Tongariro volcano, New Zealand. J. Volcanol. Geotherm. Res. 403, 106993.

Raczek, I., Jochum, K. P., Hofmann, A. W., 2003. Neodymium and strontium isotope data for USGS reference materials BCR-1, BCR-2, BHVO-1, BHVO-2, AGV-1, AGV-2, GSP-1, GSP-2 and eight MPI-DING reference glasses. Geostand. Newslett. 27, 173-179.

Robertson, E.I., Davey, F.J., 2018. The basement morphology under Tongariro National Park, southern Taupo Volcanic Zone. N.Z. J. Geol. Geophys. 61, 570-577.

Rodriguez-Navarro, C., Cultrone, G., Sanchez-Navas, A., Sebastian, E., 2003. TEM study of mullite growth after muscovite breakdown. Am. Mineral. 88, 713-724.

Rollinson, H.R., 1993. Using geochemical data: evaluation, presentation, interpretation. John Wiley & Sons, New York, 352 pp.

Rudnick, R.L., Gao, S., 2003. Composition of the continental crust. Chapter 3.1 in: Holland, H.D., Turekian, K.K. (eds.), Treatise of Geochemistry, Vol. 3. Elsevier, Amsterdam, p. 1-64.

Rudnick, R.L., McDonough, W.F., McCulloch, M.T., Taylor, S.R., 1986. Lower crustal xenoliths from Queensland, Australia: evidence for deep crustal assimilation and fractionation of continental basalts. Geochim. Cosmochim. Acta 50, 1099-1115.

Scanlan, E.J., Scott, J.M., le Roux, P.J., 2020. Pyrometamorphosed Otago Schist xenoliths cause minor contamination of Dunedin Volcanic Group basanite. N.Z. J. Geol. Geophys. 63, 530-546.

Sisson, T.W., Salters, V.J.M., Larson, P.B., 2014. Petrogenesis of Mount Rainier andesite: magma flux and geologic controls on the contrasting differentiation styles at stratovolcanoes of the southern Washington Cascades. Geol. Soc. Am. Bull. 126, 122-144.

Sissons, B.A., Dibble, R.R., 1981. A seismic refraction experiment southeast of Ruapehu volcano. N.Z. J. Geol. Geophys. 24, 31-38.

Spera, F. J., Bohrson, W.A., 2004. Open-system magma chamber evolution: an energy-constrained geochemical model incorporating the effects of concurrent eruption, recharge, variable assimilation and fractional crystallisation (EC-E'RA$_X$FC). J. Petrol. 45, 2459-2480.

Stern, T., Benson, A., 2011. Wide-angle imaging beneath an andesitic arc: central North Island, New Zealand. J. Geophys. Res. 116, B09308.

Sutton, A.N., 1995. Evolution of a large silicic magma system: Taupo volcanic centre, New Zealand. Unpublished PhD thesis, The Open University, Milton Keynes, United Kingdom, 416 pp.

Tanaka, T., Togashi, S., Kamioka, H., Amakawa, H., Kagami, H., Hamamoto, T., Yuhara, M., Orihashi, Y., Yoneda, S., Shimizu, H., Kunimaru, T., Takahashi, K., Yanagi, T., Nakano, T., Fujimaki, H., Shinjo, R., Asahara, Y., Tanimizu, M., Dragusanu, C., 2000. JNDi-1: a neodymium isotopic reference in consistency with LaJolla neodymium. Chem. Geol. 168, 279-281.

Thirlwall, M.F., 1991. Long-term reproducibility of multicollector Sr and Nd isotope ratio analysis. Chem. Geol. 94, 85-104.

Thirlwall, M.F., 2000. Inter-laboratory and other errors in Pb isotope analyses investigated using a ^{207}Pb-^{204}Pb double spike. Chem. Geol. 163, 299-322.

Todd, E., Stracke, A., Scherer, E., 2015. Effects of simple acid leaching of crushed and powdered geological materials on high-precision Pb isotope analyses. Geochem. Geophys. Geosyst. 16, 2276-2302.

Tommasini, S., Davies, G.R., 1997. Isotope disequilibrium during anatexis: a case study of contact melting, Sierra Nevada, California. Earth Planet. Sci. Lett. 148, 273-285.

Townsend, D.B., Leonard, G.S., Conway, C.E., Eaves, S.R., Wilson, C.J.N., 2017. Geology of the Tongariro National Park area [map]. Lower Hutt (NZ): GNS Science. 1 sheet + 109 pp., scale 1:60,000. (GNS Science geological map 4).

Villamor, P., Berryman, K., 2006. Evolution of the southern termination of the Taupo Rift, New Zealand. N.Z. J. Geol. Geophys. 49, 23-37.

Villamor, P., Berryman, K.R., Ellis, S.M., Schreurs, G., Wallace, L.M., Leonard, G.S., Langridge, R.M., Ries, W.F., 2017. Rapid evolution of subduction-related continental intraarc rifts: the Taupo Rift, New Zealand. Tectonics 36, 2250-2272.

Wallace, L.M., Beavan, J., McCaffrey, R., Darby, D.J., 2004. Subduction zone coupling and tectonic block rotations in the North Island, New Zealand. J. Geophys. Res. 109, B12406.

White, A.J.R., Chappell, B.W., 1977. Ultrametamorphism and granitoid genesis. Tectonophysics 43, 7-22.

Wilson, C.J.N., Houghton, B.F., McWilliams, M.O., Lanphere, M.A., Weaver, S.D., Briggs, R.M., 1995. Volcanic and structural evolution of Taupo Volcanic Zone, New Zealand: a review. J. Volcanol. Geotherm. Res. 68, 1-28.

Worden, R.H., Champness, P.E., Droop, G.T.R., 1987. Transmission electron microscopy of the pyrometamorphic breakdown of phengite and chlorite. Mineral. Mag. 51, 107-121.

Wolf, W., Romer, R.L., Glodny, J., 2019. Isotope disequilibrium during partial melting of metasedimentary rocks. Geochim. Cosmochim. Acta 257, 163-183.

Zeng, L., Asimow, P.D., Saleeby, J., 2005. Coupling of anatectic reactions and dissolution of accessory phases and the Sr and Nd isotope systematics of anatectic melts from a metasedimentary source. Geochim. Cosmochim. Acta 69, 3671-3682.

Journal Pre-proof

Journal Pre-proof

Highlights

- Metasedimentary xenoliths immersed in andesitic magmas underwent mineralogical, chemical and isotopic changes
- Compositional changes significantly affected most element concentrations and isotopic ratios except $^{143}Nd/^{144}Nd$
- Mineral breakdown (chiefly white mica, illite, chlorite and quartz) resulted in average mass losses of 50% in xenoliths
- Xenoliths were derived from the Mesozoic Kaweka and Waipapa terranes

Journal Pre-proof